
A TIME EFFICIENT TECHNIQUE TO DETERMINE THE ENTROPY COEFFICIENT OF A LITHIUM ION CELL

Caius Patel, Tom Goodwin, Tomos Williams, Aidan Watkins

ABSTRACT

Lithium-Ion cell technology is fundamental to the human future as a sustainable power source. An accelerated design process for these cells is required, yet current testing methods of newly created cell technologies only sees to stagger and hamper the process through excessive time consumption. Through two novel techniques of cell Open Circuit Voltage (OCV) feedback and thermal actuation upon the cell, accurate cell entropy coefficient determination at a given State of Charge (SOC) can be reduced from the current industry standard by 97%. The OCV feedback predicts the settling point of electrochemical voltage equilibrium point through a variable input curve fitting function. OCV feedback also shows that the settling time when a temperature step of 5°C in a time of 5 minutes. The thermal heating block is able to offer improvements by homogeneously heating the cell via surface conduction in less than 2 minutes. These techniques have proved a methodology for a determination of the cell entropy coefficient to an accuracy of 30 μ V/K with a voltage and temperature resolution of 180 μ V and 1mK respectively within a time-frame of many orders of magnitude smaller than current industry standard.



Supervised by Dr Alistair Hales
Department of Electrical and Electronic Engineering
University of Bristol
2021

DECLARATION

This project report is submitted towards an application for a degree in Mechanical Engineering at the University of Bristol. The report is based upon independent work by the candidates. All contributions from others have been acknowledged and the supervisor is identified on the front page. The views expressed within the report are those of the authors and not of the University of Bristol.

We hereby assert our right to be identified as the authors of this report. We give permission to the University of Bristol Library to add this report to its stock and to make it available for consultation in the library, and for inter-library lending for use in another library. It may be copied in full or in part for any bone fide library or research worker on the understanding that users are made aware of their obligations under copyright legislation.

We hereby declare that the above statements are true.

© Copyright, Caius Patel, Tomos Williams, Tom Goodwin, Aidan Watkins 2022

Certification of ownership of the copyright in a dissertation presented as part of and in accordance with the requirements for a degree in Mechanical and Electrical Engineering at the University of Bristol.

This report is the property of the University of Bristol Library and may only be used with due regard to the author. Bibliographical references may be noted but no part may be copied for use or quotation in any published work without prior permission of the author. In addition, due acknowledgement for any use must be made.

WORK ALLOCATION

- Caius Patel (gd18875)
 - Control System Design and Implementation
 - Box Design & Fabrication
 - Electrical & Electronic Design & Fabrication
 - Filtering and Noise Processing
 - Schematic
 - User Guide
- Tomos Williams (ld18021)
 - Thermal Modelling
 - Voltage Feedback Prediction
 - Temperature Curve Fitting
 - Voltage Probe Fabrication
 - Graphical User Interface
- Tom Goodwin (cd18266)
 - Heating Block CAD design
 - Filtering and Noise Processing
 - Graphical User Interface
 - User Guide
- Aidan Watkins (pe18860)
 - Safety Requirements

We confirm that the information on this page accurately describes our individual contributions to the project.

CONTENTS

| | | |
|----------------------------------|---|-----------|
| 1 | Introduction | 6 |
| 1.1 | Lithium Ion Batteries and their Construction (CP) | 6 |
| 1.2 | Thermal Properties of Lithium Ion Batteries(TG) | 7 |
| 1.3 | Thermal Runaway (CP) | 8 |
| 1.4 | Industry Standard of Testing for Entropy Coefficient (CP) | 8 |
| 1.5 | Improvement of Entropy Coefficient Measure (CP/TG) | 9 |
| 1.6 | Aims & Objectives (CP) | 10 |
| 2 | Thermal Modelling (TW) | 11 |
| 2.1 | Number of Heating Surfaces Required | 12 |
| 3 | System Design | 13 |
| 3.1 | Stack Design(TG/CP) | 13 |
| 3.2 | Control System Overview (CP) | 14 |
| 3.3 | Safety | 15 |
| 4 | Hardware Overview | 17 |
| 4.1 | Voltage Probe Holder (TW) | 18 |
| 4.2 | Thermal Interface Material(TG) | 18 |
| 4.3 | Peltier Elements(CP) | 18 |
| 4.4 | Motor Driver(CP) | 19 |
| 4.5 | Thermal Fuse(CP) | 19 |
| 4.6 | Thermistors(TW) | 19 |
| 4.7 | Adafruit ADCs (CP) | 21 |
| 4.8 | Raspberry Pi (CP) | 22 |
| 4.9 | Water Cooler (CP) | 22 |
| 5 | Design Optimisation | 22 |
| 5.1 | Filtering and Noise Processing (CP) | 22 |
| 5.2 | Voltage Feedback(TW) | 25 |
| 6 | Implementation | 26 |
| 6.1 | Final Design(CP) | 26 |
| 6.2 | Controller(CP) | 28 |
| 6.3 | Overview of a Test Cycle(CP) | 29 |
| 7 | Results and analysis | 29 |
| 7.1 | Thermal Rise and Fall Time(TG) | 29 |
| 7.2 | Voltage Settling Time Determination(TW) | 30 |
| 7.3 | Time Efficient Accuracy of Entropy Coefficient Determination (TG/TW/CP) | 31 |
| 8 | Discussion | 33 |
| 8.1 | Design Comparison(CP) | 33 |
| 8.2 | Design Limitations(CP/TW) | 33 |
| 9 | Conclusion (CP) | 34 |
| 9.1 | Areas of Future Research & Development(CP) | 35 |
| Acknowledgements | | 36 |
| References | | 37 |
| User Guide(CP/TG) | | 39 |
| Complete Schematic(CP) | | 39 |

| | |
|--|-----------|
| User Interface Manual | 41 |
| Appendix A - Code Structure Flow Diagram (TG) | 44 |
| Appendix B - Code Structure(TG) | 45 |
| Overview | 45 |
| EntropyCoefficient.py | 45 |
| controlPeltiers() | 45 |
| Predict() | 45 |
| system() | 45 |
| Appendix C - Apparatus Diagrams (CP) | 51 |

1 INTRODUCTION

Lithium Ion batteries are becoming ever more common in our daily world. Over the past few decades, an increase in their use for energy storage within portable consumer devices such as phones to larger scale HEVs and EVs [1], has consequently put them at the forefront of electrical energy storage [2,3]. Looking to the future, the technology behind Lithium-ion batteries needs to be understood in order to create more energy-dense, robust and reliable batteries [4], whilst also managing the cells in order to maximise their potential.

An increase in implementation across sectors has led to the cells being subject to more thermal and electrical stresses which need to be understood [5]. These stresses, in particular the thermal boundary conditions which a cell experiences, have a strong correlation to the characteristics of the cell by affecting the lifetime and performance [6,7].

With this ever increasing demand, the new and developing technologies need to be understood and tested within a reduced time frame. For industrial applications it is advantageous to have a simplified and quicker method to model and test cell characteristics [5].

1.1 Lithium Ion Batteries and their Construction (CP)

Lithium ion battery packs are typically found in many applications such as EVs and HEVs. These battery packs are comprised of a large number of cells arranged in series and parallel configuration. For this experiment, only individual cells are investigated.

The three main types of lithium cell are prismatic (Figure 1), cylindrical (Figure 2) and pouch cells (Figure 3). Each have their own benefits; the prismatic and the cylindrical have higher mechanical stability, and the prismatic and pouch cells have higher packaging and energy density. The cylindrical cell, is however the most commonly available cell due to low manufacturing costs. As its use is widespread across power tools and EVs, this paper will focus on developing a methodology and understanding for these cell types.



Figure 1: Prismatic Cell -
Typically Used in Small
Gadgets



Figure 2: Cylindrical Cell -
Tesla Cell Used in EV
Battery Modules



Figure 3: Pouch Cell -
Typically Used in Drones and
RC Applications

Cylindrical cells come in three standard sizes: 18650, 21700, 26650. These refer to the dimensions of the height and diameter of the cell: an 18650 cell has a 18mm diameter and 65mm height. Tesla currently use 21700 cells due to an increase in energy density of around 50% against the average 200 kWh/kg of their 18650 cell [8]. Studying how these cells behave under differing thermal stresses at varying states of charge, allows for more efficient use of their energy by the cell management system (BMS) and hence an increased range of their EVs.

Current lithium ion cells are comprised of an anode and cathode based off insertion-compounds with an organic electrolyte which carries the Lithium salt [9]. These are separated by a membrane and solid electrolyte interface (SEI) which only allows for diffusion of ions through it, see Figure 4. During charging and importantly the discharge process, the ions flow from the lattice structure of the anode (typically graphite [10]) to the cathode, producing current. The lithium atoms release their electrons and flow through the SEI, pushing the electrons to the cathode via an external circuit. This allows for electrical work to be extracted from the chemical store in the cell.

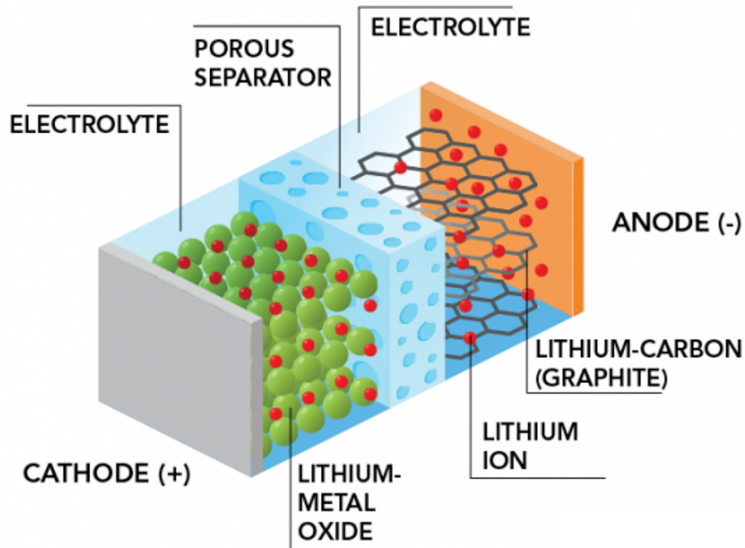


Figure 4: Structure of a Lithium Ion Cell [11]

Degradation occurs through ions becoming irreversibly bonded to the anode compounds, overall reducing the capacity and performance of the cell [6, 12]. When electrochemical stresses are applied to the cell, large fluctuations cause loss of lithium ions to the SEI. This is due to the SEI fracturing and degrading, a dominant mechanism of cell capacity loss [13].

Bonding of lithium to the anode and pulverisation of the SEI occurs during overcharge and high thermal stresses. It is the responsibility of the BMS to control the charging and discharging rates of the cell, optimally reducing the effects of these external thermal and electrochemical stresses in order to preserve cell performance. An accurate thermal model of the cell is required to regulate the cell effectively.

1.2 Thermal Properties of Lithium Ion Batteries(TG)

The total heat energy generated by a lithium ion cell is represented by an expression derived by Thomas and Newman [14]. The first term of the equation represents the resistive losses associated with the cell, the second term is the effects of change in entropy of the cell (which are reversible), while the third term represents heat generated by chemical reaction, the fourth is the heat due to mixing. For industrial grade cylindrical lithium ion cells the 3rdrd and 4th terms, which are both irreversible heat generation, can be neglected [15]. This leaves only the ohmic losses and the reversible heat term, the latter is the entropic heating term that this investigation concerns itself with.

$$\dot{Q} = I(V - U^{avg}) + IT \frac{\partial U^{avg}}{\partial T} - \sum_i \Delta H_i^{avg} r_i - \int \sum_j (\bar{H}_j - \bar{H}_j^{avg}) \frac{\partial c_j}{\partial t} dv \quad (1)$$

Ohmic heating is trivial to calculate for any cell given that accurate voltage and current sensors are in place, however the entropic heating requires the entropy coefficient to be known accurately. Where entropy coefficient refers to the partial differential in the second term. In order for a BMS to realise

these temperature induced voltage changes of entropic heating, it is vital to have accurate values of entropy coefficient [16, 17].

During charging and discharging cycles the cell undergoes reversible and irreversible energy changes [18]. The effects of irreversible heating remain low during low discharge rates [15] however when subject to higher discharge stresses they cannot be ignored. Irreversible heating are thermal losses which occur throughout the cell, however the reversible entropic heating is of greater significance as usable energy can be extracted.

1.3 Thermal Runaway (CP)

Thermal runaway can cause cells to exothermically decompose exponentially and catch fire and poses a serious safety risk. There have been numerous instances of thermal runaway of cells in the commercial world, with the majority having catastrophic impacts. Lithium Ion cells in particular are prone to this. Typically, thermal runaway occurs due to changes in the electrochemical balance and in rare cases, due to an internal short in the cell. Usually is as a result of thermal or electrical stresses in the form of charging or discharging, especially when at extremes in temperature [19].

The propagation for thermal runaway is related to the Arrhenius form, which states that as the temperature increases the rate of decomposition increase exponentially and thus so does the self-heating rate. This Arrhenius form explains how thermal runaway can be so dangerous as the reaction can escalate rapidly [20].

Elevation in temperature of the cell causes exothermic decay within the cell. In a cyclical process of positive feedback, the decay causes an increase in the cell temperature which in turn causes a further exponential increase in decay [21]. Once the stability of the cell has been compromised, the remaining thermal and electro-chemical energy will be violently released into the surroundings via explosion.

1.4 Industry Standard of Testing for Entropy Coefficient (CP)

The entropy coefficient is defined as the change in cell voltage due to a change in temperature at a certain state of charge. Hence entropy coefficient can simply be defined as the dV/dT . Lenz et al [5], derives a simplified entropy coefficient given in Equation 2.

$$\varepsilon(SoC) = \left(\frac{\delta V_{oc}(SoC, T)}{\delta T} \right) \Big|_{SoC} \quad (2)$$

Determination of the entropy coefficient of the cell can be carried out in a various ways, these are laid out in Doh et al [22]. The two main ways used in industry to measure entropy coefficient are:

- Potentiometrically
- Caliometrically

Caliometric measurements to calculate the entropy coefficient require the cell to be charged and discharged. At low charge and discharge rates the irreversible energy for charge and discharge are equal and negligible [15]. As the reversible energy represents the entropy coefficient, the balance when subtracting the two heat flows can be converted to the entropy coefficient. However this requires complex data processing to occur due to a time delay from nominal cell temperature and the temperature at the sensors.

Potentiometric entropy calculation is the most common procedure in industry. As the entropy coefficient is a function of Temperature (T) of the cell at a given State of Charge (SOC), SOC must be held at a constant while the temperature is varied. Through a method laid out by Bazinski et al [23], the state of charge is held at a constant while the temperature of the cell is stepped at regular intervals. Once a cell is charged to a certain SOC it is left for a minimum period of 4 hours to ensure the cell has reached electrochemical equilibrium and there is no change in cell chemistry [24]. Heating occurs within a climate chamber to gradually heat the cell to a homogeneous temperature [17, 25]. Again

the cell is left to come to equilibrium before Open Circuit Voltage (OCV) of the cell is read. This is illustrated in Figure 5. From the step change in temperature, the change in voltage can be calculated and the entropy coefficient calculated.

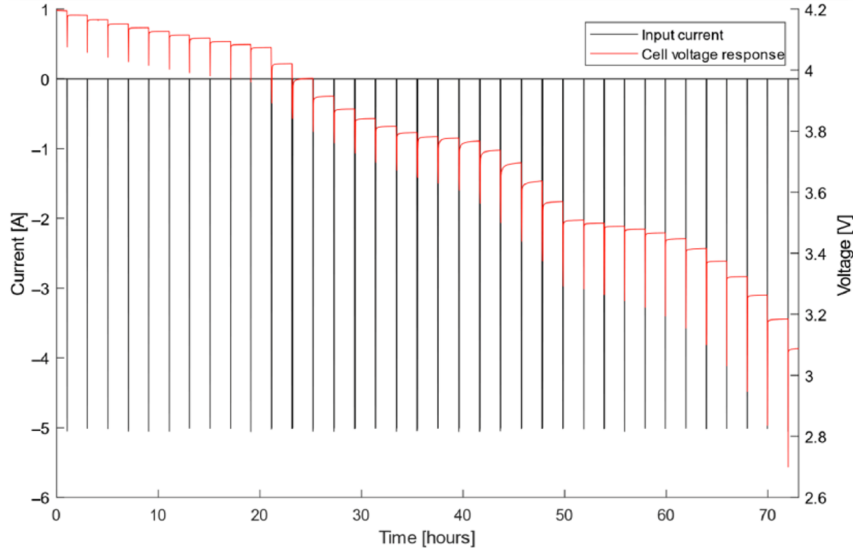


Figure 5: Measured Voltage as Cell is Discharged

Easily the largest issue with the current industry standard of testing is the long test duration. The time taken to test an average cell can vary between 6-17 days [26], in cases tests can take 11 days for thermal cycling [27] and this doesn't account for cell relaxation periods during SOC changes. Furthermore, cells will self discharge over time, the longer the test the more the cell will discharge. This only yields less accurate results as the SOC doesn't remain constant, as a result data processing has to be implemented to account for the drop in charge level.

During the heating process, the climate chambers heat the cell via convection which only adds to total heating time. Furthermore, homogeneous temperature is required from the cell [17, 25] to give accurate results. The current way of measuring entropy coefficient is not sustainable for continued use, purely based on how long measurements of entropy coefficient take.

1.5 Improvement of Entropy Coefficient Measure (CP/TG)

A potentiometric method is clearly optimal to measure the cells as it offers more accuracy and reliability. Moreover, as thin cylindrical cells are being tested, potentiometric methods offer more accurate results than caliometric methods as the cells are thinner [18].

Identification of thermal cycling needs to be improved. Whereby, both heating and cooling of the cell can be carried out more efficiently via thermo-electric cooling, demonstrating better performance [17, 25, 28]. In general conductive heat transfer allows for far greater rate of transfer of energy than convective methods. It reasons that therefore the method of heat transfer represents one of the key areas were time reductions can be made. However despite this the convective method is popular, as multiple batteries may be tested simultaneously which offers a practical and scientific advantage over current conductive methods. However, should a conductive device which also allows parallel testing be manufactured, it could be a highly desire-able device in the lithium-ion cell sector.

The long periods of time after each charge/discharge can also potentially be reduced. These periods are usually four hours long and are there to allow for the cell to reach electrochemical equilibrium, meaning that the voltage has stopped changing. Although four hours after a charge/discharge the rate of change in voltage will have reduced significantly, theoretically it is still not zero and the voltage drift will effect entropy coefficient measurement. Osswald et al. demonstrated that even after 24 hours of voltage relaxation the change in voltage is measurable [5, 17, 29–31]. They also showed that

the voltage drift can be accounted for in the entropy coefficient, not only after 24 hours of relaxation but even for periods as low as 30 minutes. By simply measuring the voltage drift for 20 minutes a quadratic curve can be fitted to the voltage drift, based on which the subsequent experimental voltage measurements can be offset accordingly. Osswald et al. demonstrated that this method can allow accurate measurement of entropy coefficient with minimal relaxation time.

Mendoza et al. [30] optimised the temperature step profile to reduce overall test time. Instead of stepping temperature discretely a continuous function was found to be optimal, and it was able to produce an a measurement of an entropy coefficient at a single SOC in 2 hours. This is a particularly large decrease from the industry standard length of 15-24 hours as convective cooling was used. However Mendoza et al. were unable to measure the entropy coefficient as accurately as was done by Forgez et al. [15]

1.6 Aims & Objectives (CP)

The overall objective of the design project is to reduce the time taken to measure the temperature induced voltage change within the cell. This is how the entropy coefficient will be determined for any state of charge. In order to achieve these overarching goals, the aims are to:

- Measure the entropy coefficient of a LG M50 cell at a given state of charge
- Achieve an entropy coefficient accuracy of $1\text{mV}/\text{K}$ by measuring voltage at a resolution of $100\mu\text{V}$ and temperature at a resolution of 0.01K
- Heat the cell homogeneously through a thermal interface to reduce the cell heating time
- Compared to the industry standard of 4 hours per step, reduce the time taken to heat the cell by greater than 50%.

The first priority of the experimental apparatus is to measure the cells entropy coefficient. In order to be comparative to existing literature and current methods of testing within the industry, a desired entropy coefficient (mentioned above) is required to a certain accuracy.

Furthermore, to offer a significant improvement over the current industry standard, the design aims to tackle the current issue of long experiment times. Due to the lengthy experiments that occur within industry, a need to improve this time is evident. The second main aim of the design is to measure the entropy coefficient in a time frame which is far greater than that of the current.

These aims allow for development of a user friendly and robust method of testing the entropic heating coefficient of a cell in a time efficient manner. The experimental process will be significantly faster than the current industry standard whilst also maintaining a similar degree of accuracy. For greater insight into the design, see Section 1.6.1 for the design specification.

1.6.1 Design Specification

In order to achieve these aims, a design specification for the experimental apparatus can be created. It aims to focus on both the physical design and its capabilities for measuring cell characteristics. The design specification is listed below:

- Apply sufficient heating power of 50W
- Heat the cell homogeneously in 30 minutes
- Heat/cool the cell from 5°C to 40°C in 5°C increments
- Measure the cell temperature to 0.01°C of accuracy
- Measure cell voltage to an accuracy of $100\mu\text{V}$
- Measure Entropy Coefficient to a resolution of $1\text{mV}/\text{K}$
- To be able to predict the voltage equilibrium point
- The apparatus requires a Graphical User Interface (GUI) to run and display real time results of the experiment
- Design needs to be enclosed, standalone and portable
- The test rig should be able to easily sit atop and within a lab desk.
- User guide needs to be produced to inform the user of apparatus function

2 THERMAL MODELLING (TW)

By creating a model of the heat transfer through a heating block that contains the cell, design choices can be made. It will be possible to verify whether it is viable to use conductive heat transfer to raise the temperature of the lithium ion cell.

The block is defined as an aluminium block surrounding a lithium ion cell with the ends left open for voltage connections. It is modelled in 2D as a square that surrounds a circular cell. The boundary conditions of the surface of the cell are used to understand conduction throughout the cell and further the conduction rates required by the block.

This was done by creating a partial differential equation solver in MATLAB. The model only has to be a 2D model due to the assumption of the cell and block being axially symmetric. The cell chosen for this was a 21700 cell and assumptions of the physical and thermal properties are based upon existing literature, but as the literature shows varying values for different cell constructions and chemistries, values in Table 1 were used.

| | Aluminum | Lithium-Ion Cell |
|---|----------|------------------|
| Density, kg/m^3 | 2700 | 2880 |
| Heat Capacity, $\text{K}/\text{kg K}$ | 900 | 1000 |
| Thermal conductivity, $\text{W}/\text{m K}$ | 237 | 1 |

Table 1: Thermal Properties for Simulation

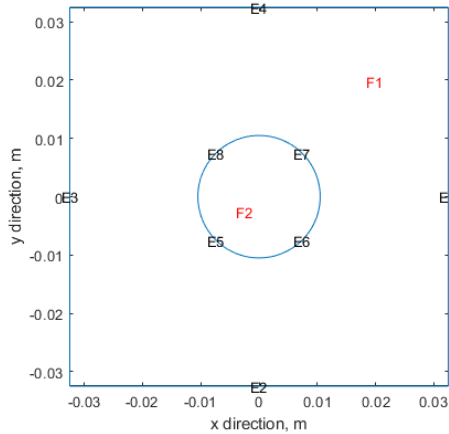


Figure 6: Setup of the Thermal Model

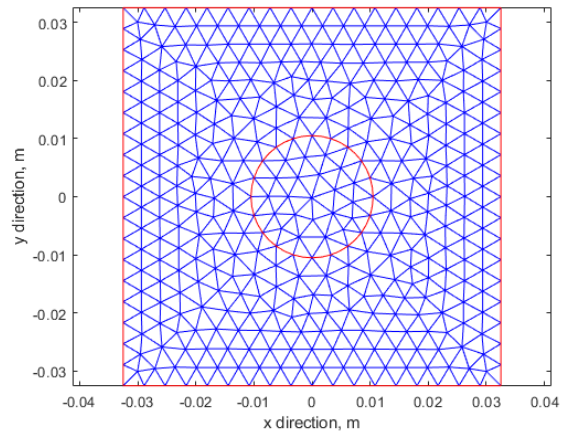


Figure 7: Mesh of the Model

Figure 6 shows the setup of the thermal with edges E1,E2,E3,E4 being the edges of the heating block that can have their temperatures changed. With the face F1 being the aluminium surrounding the face of the cell F2. Figure 7 shows the mesh used for the simulation.

The radial heat transfer coefficient varies from $0.2\text{W}/\text{mK}$ [32] to $3.6\text{W}/\text{mK}$ [33] but a value in the middle of the range of $1\text{W}/\text{mK}$ was used due to as a standard for thermal models across the industry. Further the specific heat capacity of 1000 J/kgK was used in the model and cell density was calculated using the mass and the volume from the given dimensions.

The thermal model has an ambient temperature of 25°C which is applied to all sides of the surface of the block. Drawing conclusions from the thermal diffusion shown in Figure 8, the surface of the block is simulated to have a rise time of 53 seconds to 99% of the final temperature value. This is to model a realistic thermal application because the temperature cannot instantly rise to the desired temperature. The surface temperature of the cell reaches the final value at 70 seconds, with the temperature of the inside of the cell reaching 99% of the final value at 303 seconds. This gives a rise time of the centre of the cell a lag of approximately 4 minutes compared to the surface of the cell.

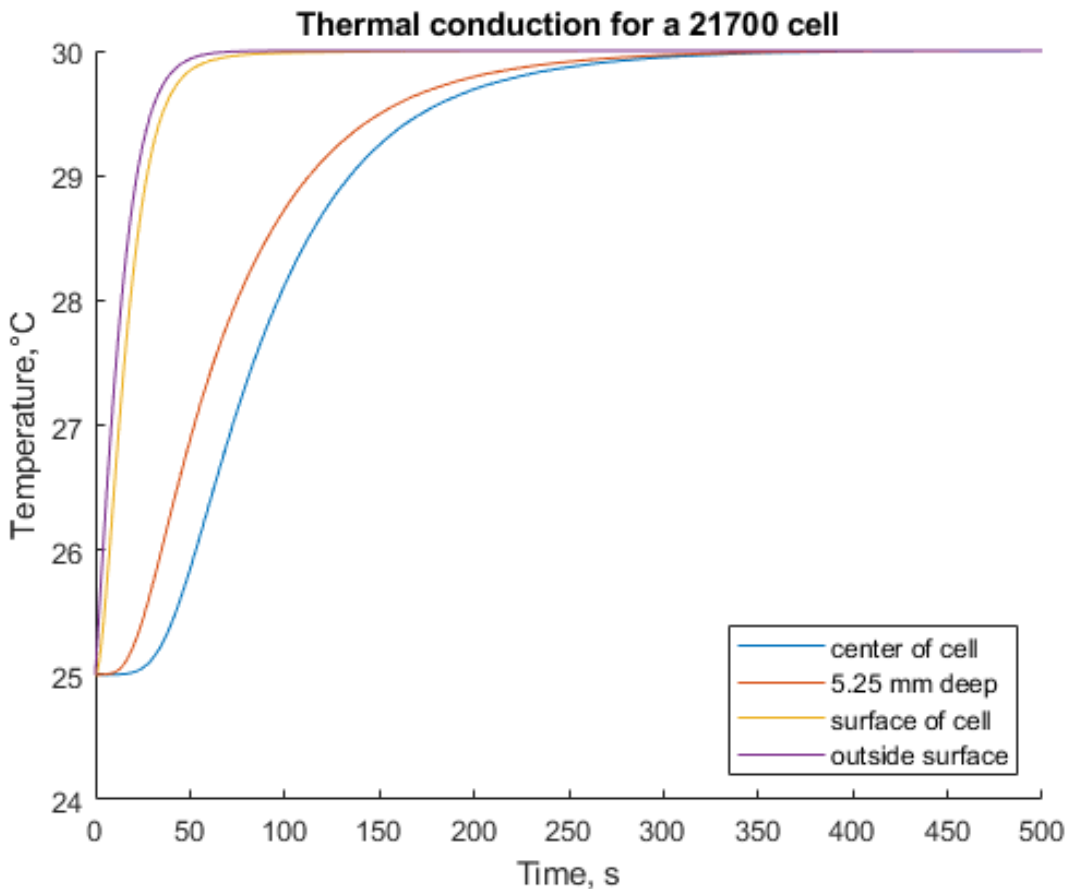


Figure 8: Thermal Diffusion Throughout the Heating Block and the Cell

This thermal model has a similar rise time to that of Osswald et al. which was shown experimentally that the lag between the surface of the cell and the centre of the cell for a 5°C rise [31] was observed to be 5 minutes. This experiment was done with 18650 cells that had a thermocouple inserted into the centre of the cell.

The difference between the experiment in Osswald et al. when compared to a thermal model is that any thermal interfaces are modeled to be ideal while in reality there will need to be a layer of thermal interface material. The thermal interface materials are normally very thin (less than 1mm) and can typically have thermal conductivities between 1 – 20W/mK. In application, a thermal interface material of minimal distance and maximum conductivity would be ideal.

There are also inaccuracies with the thermal conductivity of the cell. The assumption is just for the can of the cell and doesn't include the thermal resistance of the insulating material around the outside of the cell. This material is also very thin (roughly 0.5mm) and would put the overall thermal conductivity for the cell closer to that of Bhundiya et al. [32] as thermal conductivity was measured including the cell wrap. However, this material cannot be removed as the cell can is the negative terminal and is meant for electrical insulation as there is a risk of shorting with the positive terminal at the top of the cell. Modelling with the insulating material on the can allows for a more practical approach of a cell during testing.

2.1 Number of Heating Surfaces Required

Conductivity of the block was considered in the model. More specifically the thermal boundary conditions of the sides of the block and whether applying heat to all 4 sides was necessary. Through investigation into application of heat of 2 vs 4 sides, minimal difference in thermal gradient across the cell was seen. This is due to the aluminium having a much higher thermal conductivity than the cell, meaning the edge of the cell is isothermal. While a faster rise time of the temperature of the cell

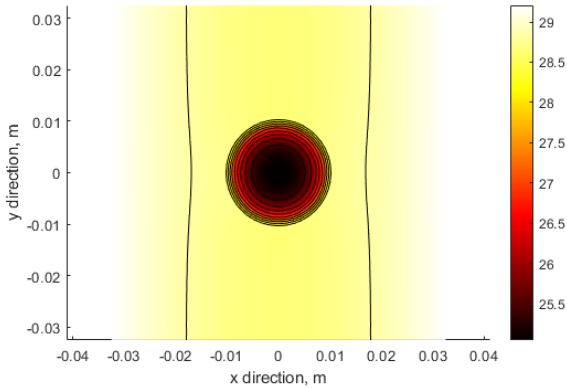


Figure 9: Thermal Simulation with 2 Edges
Heated

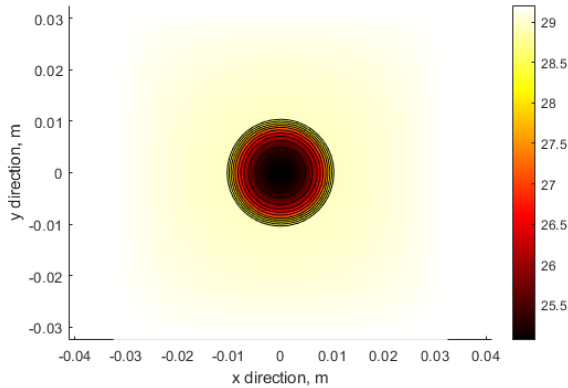


Figure 10: Thermal Simulation with 4 Edges
Heated

could be achieved using heating on all 4 sides due to more energy transfer, this would require a more complicated design of the block to allow batteries to be inserted for testing, while also increasing the cost due to having more heating elements and more control electronics. As a result heating elements are only required on 2 opposing sides to provide adequate homogeneous heating to the cell via the block. See Figures 9 and 10.

3 SYSTEM DESIGN

The system design provides an overview of the key actuation systems which work to carry out an entropy coefficient experiment. The two main areas of the apparatus consist of the actuation stack design and the controlling systems around it.

3.1 Stack Design(TG/CP)

The cell-holders were designed and so that they could be assembled in a stack (Figure 11). The four bolts guide the cell-holders so that they are aligned correctly, and also allow other components like the cooling block and peltiers to be secured easily. Another advantage of the bolts is that the compression of the stack can be adjusted, by applying torque to the wingnuts, so that it is even and appropriately compressed. The compression of the stack is detailed in Section 4.2.

The stack was split into two sections to allow easy assembly. Furthermore, due to only requiring two heating modules (Peltiers) on opposing sides, these could be located at the top and bottom of the stack. As the stack also undergoes compression, the thermal interface material located within the semicircles of the block compress onto the cell surface. As pressure is applied and the interface material deforms. There must be space between the blocks to allow for the thermal interface deformation and so the surface of each block on semicircle side were milled down. The total segment of the semicircles are approximately 178° to allow for this compression to occur without hindrance.

There are holes throughout the aluminum block to allow for thermistors to be placed to make sure the block is being heated homogeneously, thermistors will also be able to be placed in-between the thermal interface material and the surface of the cell and the thermal interface material and the peltier elements. This makes it possible to make sure that the cell is being heated homogeneously.

The two materials considered for the stack are copper and aluminium. The material of the stack chosen is aluminium. Whilst copper offers a higher thermal conductivity, due to being more dense, the specific volumetric heating capacity of aluminium is greater. Therefore the thermal diffusivity through aluminium is greater and the block will be more responsible to temperature changes. Furthermore aluminium is easier to machine and is the cheaper of the two options.

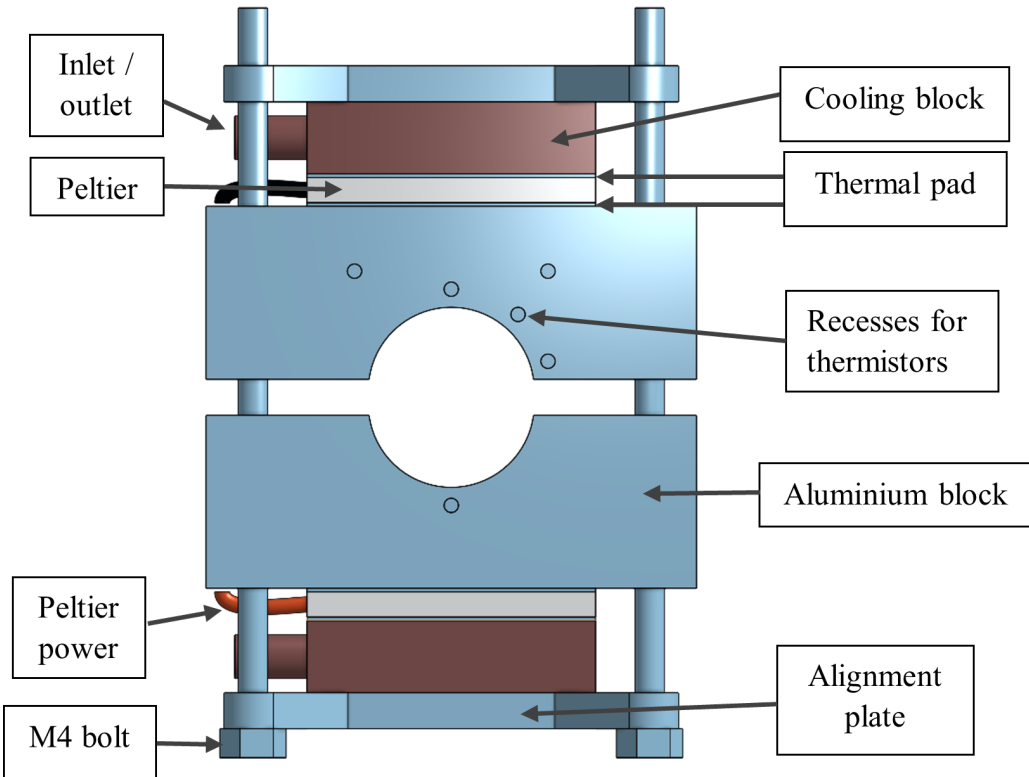


Figure 11: 21700 Cell Thermal Block Setup

3.2 Control System Overview (CP)

The main purpose of the control system is manage the thermal cycling of the cell, creating profiles and data allowing for extraction of the entropy coefficient.

The thermal changes that occur throughout the block are actuated by the peltier elements. These both heat and cool the cell to our desired temperature at the cell surface. As shown through the thermal modelling of the paper and through Osswald et al. [31], holding the cell surface temperature at a constant will allow the cell to become homogeneous over a period of time.

Thermal stepping will occur each time the cell has shown characteristics of thermal and electrochemical equilibrium. These are detailed later in this report and will be based off of a cell voltage feedback loop. Once desired values of the cell voltage have been met, the control system will move onto the next step. Stepping over a range of thermal values will allow for cell characterisation and determination of the entropy coefficient.

The two main control systems outlined above which are at the projects core are:

- Peltier Control Loop
- Voltage Feedback Loop

The control loops have been shown in block model format through Figure 12. The control signals are sent from the Raspberry Pi to the actuation system of the motor driver and peltier cooling modules. These in turn affect the cells thermo-electrochemical potential via the heating block. Feedback signals of voltage and temperature are then sent back into the Raspberry Pi to form a closed loop system.

A controlling algorithm is applied to the feedback signals. The aims of which are to provide a fast but stable rise to the desired cell surface temperature. At which point, the cell will be held at the desired temperature until the voltage sensing system detects that the OCV has equalised and electrochemical potential has read equilibrium.

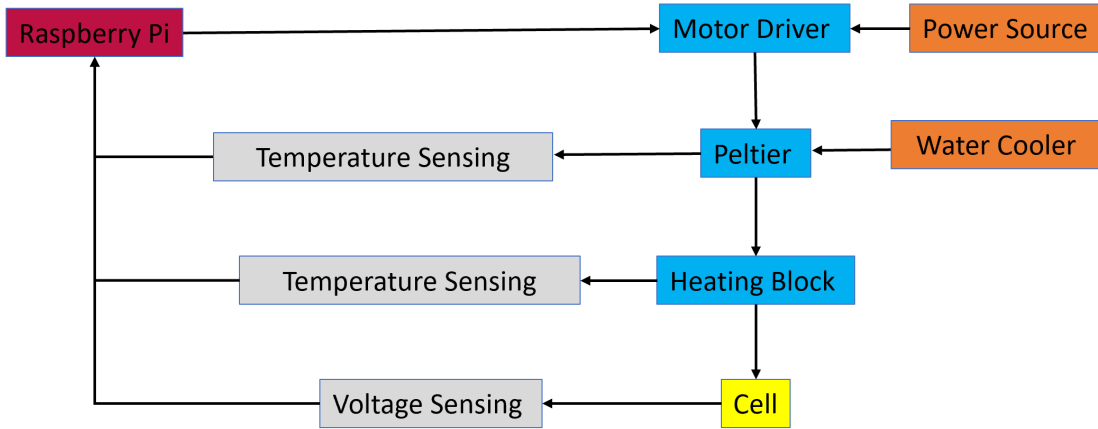


Figure 12: Block Model of the Control System

3.3 Safety

3.3.1 Safety Requirements (CP/AW)

In 2006 there were a variety of reports of phone and notebook batteries exploding, in almost all of these cases the explosions were due to thermal runaway. This highlights the fact that there exists very present and real risks if appropriate risk mitigation is overlooked.

Safety considerations are of paramount importance, especially in regards to experiments where heat is applied to cells and there is potential for electrical fires. A variety of mechanical and electrical safety measures have been implemented throughout the project. A rigorous risk assessment was carried out during the design process of the project. A multitude of varied risks were identified thus meaning that appropriate action had to be taken to mitigate those risks.

The safety concerns identified are detailed below:

- Cell explosion
- Electrical fire
- Electrical shorts (via coolant)

There are a variety of reasons that can cause a cell to explode, a majority of these risks are associated with charging the cell. These require mitigation.

As previously mentioned there are a few mechanical or thermal failures which act as triggers for thermal runaway. It can be due to electro-chemical abuse to a cell in the form of over charging or over discharging. Further charging or discharging at either too high or too low temperatures can also kick start the rapid exothermic decomposition. There is also the possibility of an unprovoked short circuit within the cell which in turn leads to thermal runaway.

Another risk to consider is the mixing of liquids and electronics. When pumping a liquid in the vicinity of electronics there is a risk of an electrical fire therefore the coolant poses two potential problems. There is potential for the coolant to spill and leak out of the tubing, this can lead to both an electrical fire and also poses a potential slip hazard to the user if the coolant were to get onto the floor.

3.3.2 Risk Mitigation(AW/TW/CP/TG)

Much of risk associated with cell fires and explosions is present when the cell is being charged or discharged, therefore the lack of a cell-cycler within the experiment avoids many potential risks. To minimise impacts of a failure risk mitigation can be implemented as either active or passive.

In practice, when experimenting with lithium cells, a safe crate should be allocated to enable safe dispose of a cell. Cells should also be stored in the fridge as to keep the internal electro-chemical reactions in the cell at a low rate and further handled delicately when installing them into experimental apparatus.

To minimise the risk of thermal runaway, the cell should not be heated above 50°C. This should be implemented via software as an active limitation on the system. However in the case of failure of a software issue, a human intervention mechanism of a kill switch can shut off the experiment and allow it to safely cool. In a passive mitigation, a mechanical thermal fuse can be installed to cut supply power to the experiment. In this way an software control, mechanical and human intervention provide redundant safety.

Shorts can occur externally within the cell though coolant. Hence, electrical and liquids should be kept as separate possible to minimise the potential failure effects. Internal shorts of a cell are latent causes for thermal runaway, and in the worst case scenario, passive mitigation must consider a cell fire or explosion. In this case an enclosure is required to withstand any potential damage. It should also be able to increase the time available to react in order to deal with a failure in the case of an emergency.

3.3.3 Enclosure(AW)

Whilst it is important to have a variety of measures in place to prevent a risk developing it is also vital to have measures in place that can handle the most catastrophic of outcomes. Therefore it is important to have a casing for the kit that is robust enough to withstand the most catastrophic of outcomes. In order to do this first an appropriate material for the housing must be chosen.

| Material | price per cm^2 | heat resistance | explosive safety | ease of assembly | insulation properties |
|---------------------|--------------------------------------|--|--|--|--|
| aluminium extrusion | 3.7 p | 1260C (loses half of structural integrity at 600) | below 600C very good | comes pre made only requires the apparatus to be fit inside it | good conductor therefore increase in heating times but reduction in cooling times |
| polycarbonate | 0.023-0.044p(3mm-6mm) | will withstand burst at 1116C, or several hours at 260C | has higher tensile strength than acrylic however loses toughness at 140C. 10,000 psi | would require cutting a large piece into several panels to form a box, then either melted together, bolted or clamped. Can be brought pre-fabricated | mildly insulating, less so than acrylic particularly as thicker acrylic would be needed to provide equivalent tensile strength |
| wood | 0.35p | would catch fire, MDF could release toxic fumes depending on glue used | could splinter and cause more of a hazard, tensile strength is unpredictable as different sheets of wood would have different strengths, neither plywood or MDF would be appropriate | would require cutting up a board to size and forming a box using screws as many glues are not heat resistant | medium levels of insulation |
| acrylic | 0.018-13.9p(3mm thick to 10mm thick) | will deteriorate badly at 160C | 100mm thick is very resistant to impact however heat does lower the tensile strength. 9,500 psi | would require cutting a large piece into several panels to form a box, then either melted together, bolted or clamped. Can be brought pre-fabricated | Is a highly insulating plastic especially at 10mm so would save energy during heating phase but impede the cooling phase. |
| 3d print | free(hackspace) | High heat resistance filaments have resistance of 120C | Depends partially on the infill percentage, however a polycarbonate filament is the strongest that is readily available, is still weaker than the pre fabricated sheets of PC | Easy to make to the exact size requirements for our purposes | again depending on the infill percentage the insulation will change but it will be less so than the PC |
| perspex | 0.78p | melts at 160C | comparable to polycarbonate, however harder to find at thicknesses beyond 3mm 9,800 psi | can be brought pre-fabricated | less than PC |

Figure 13: Comparative Analysis of Housing Materials

The casing for the cell test kit must be able to safely withstand the worst case scenario of the cell

test kit failing, this mainly includes being able to contain a fire and explosion. There are a variety of options that can be considered, the choice ultimately comes down to where the priorities of the project lie.

Given that a single stand-alone experimental device is being made then safety, functionality and simplicity are of high priority. Cost of materials, easy of assembly and optimisation for space are all considerations more relevant to mass production, and therefore have a low impact on the choice of material. As safety is the priority the strength of the materials will be considered.

Although tensile strength and fracture strength are not equivalent, they do have a strong correlation. The fracture strength of a material is usually only marginally lower than the static tensile strength so still provides a reliable frame of reference and as the tensile strength of a material is much more readily available than the fracture strength it is a reasonable metric to choose.

Taking into consideration the table of materials 13 and the design requirements, the most appropriate choice for the casing is poly-carbonate as it is a cost-effective method that has the highest tensile strength and can withstand high temperatures for short periods of time which is what is required. It also has the added benefit of being transparent, enabling any potential cell failures to be spotted.

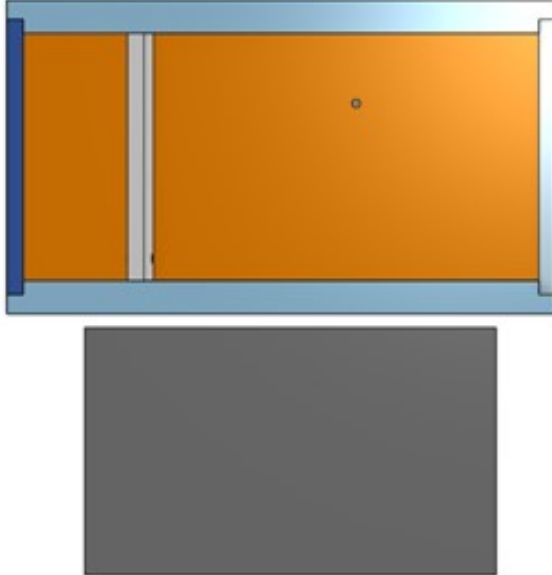


Figure 14: CAD Design for the Cell Testing Housing

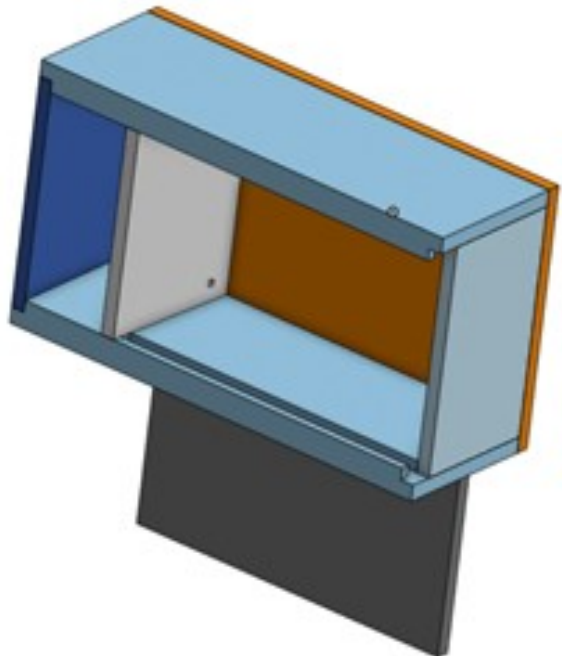


Figure 15: Alternate View of the Housing

For the physical design of the housing there have been considerations made, primarily having a separate section so that the electrical system is separated from the heating apparatus. Seen in Figures 14 and 15. The reason for this is to ensure that the electrics operate at a cool optimal temperature during the experiment. Furthermore, if there is a coolant leak, the compartmentalised sections should prevent liquid-electrical shorts.

4 HARDWARE OVERVIEW

The hardware overview is comprised of the main components used in the design to carry out the experimental process. Together these form the control systems which determine, actuate, read and feedback temperature and voltage of the cell.

4.1 Voltage Probe Holder (TW)

For making good connection with a lithium ion cell spring loaded pins were used. A holder was designed to allow the probes to be moves horizontally to allow for good connection and vertically to allow for the connection to be made in the centre of the cells tabs. The design shown in Figure 16 was laser cut and assembled. Figure 17 shows the final assembly of the battery holder. The pins allow for both a voltage and current connection to be made. This would allow for the cell to be charged and discharged using either a cell cycler or a load bank, and the voltage to be measured simultaneously.

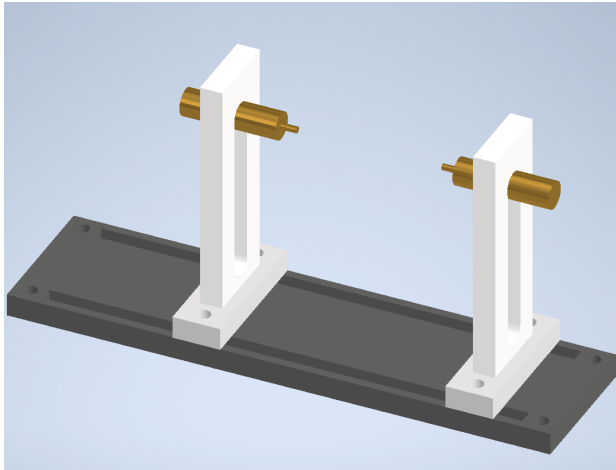


Figure 16: Design of Voltage Probe Holder

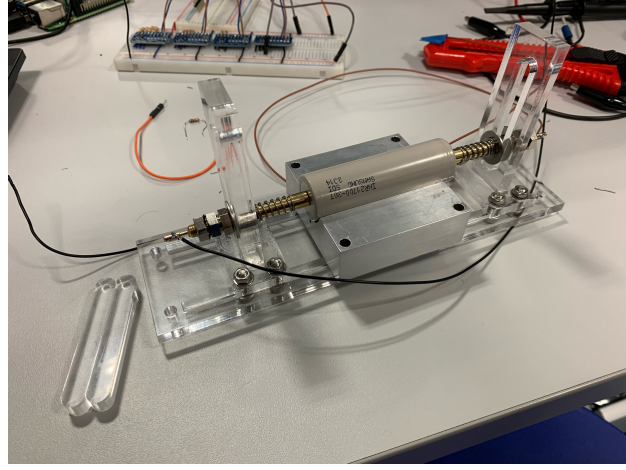


Figure 17: Picture of Constructed Voltage Probe Holder

4.2 Thermal Interface Material(TG)

The thermal interface between components is of great importance as it is optimal to maximise the heat transfer from peltier to the cell via heating and cooling block. Thermal interface material improves surface contact which reduces the thermal contact resistance as the space between the two surfaces is filled by a conductive material rather than air, which is generally a few orders of magnitude less conductive. Whilst thermal interface's have higher conductivity than air, they have a lower conductivity than aluminium, so too much thermal interface can decrease overall conductivity.

To achieve maximum conductivity liquid thermal paste is preferred to the solid thermal pads as it can be applied so that minimal additional material is placed between the surfaces, whereas thermal pads have a set thickness. However, thermal paste is difficult to use practically as it can spill and create mess, and it would have to be re-applied every time the cell was removed from the holder, which would take a lot of time. It was decided that the thermal performance increase by using thermal paste over pads was not significant enough and so thermal pads were chosen.

Thermal pads chosen offered a thin 1.6mm interface between any thermal component. Pressure of $20N/cm^2$ is applied to the pads via the stack design, where top down pressure is adjusted via 4 wing nuts, each respectively torqued down to $1Nm$.

4.3 Peltier Elements(CP)

Adaptive peltier cooler modules (ET-161-12-14-E) were used to heat and cool the cell, see Figure 18. The temperature difference across the peltier is determined by the current passed through it. A constant 10V was applied across the peltier and current was fed via pulse width modulation (PWM) signal from the motor driver.

When comparing DC current supply over duty cycle control, the peltiers are far more inefficient when controlled through PWM. This is due to the I^2R losses within the driver when heating; a DC current supply would reduce the response time by 20-30% [34]. However, controlling a dc current supply is

more complex to implement than applying a time varying PWM signal. Since the heating block acts as a thermal capacitor between the peltiers and the cell, PWM control is adequate.

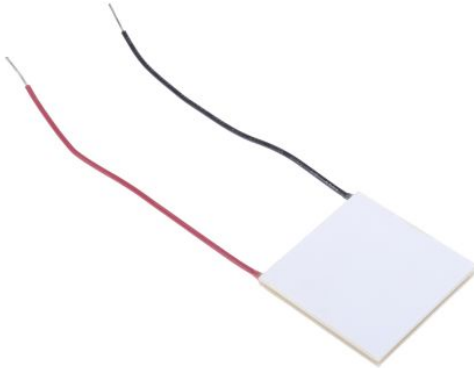


Figure 18: 40mm x 40mm 62.3W Adaptive Peltier Module



Figure 19: Cytron 10A Dual Channel Motor Driver for Peltier Elements

4.4 Motor Driver(CP)

A 10A Cytron dual channel motor driver (Figure 19) was used as a dual channel PWM amplifier. Both direction (polarity) and duty cycle could be easily controlled allowing for easy heating and cooling via software. While the PWM driving signal is inefficient for the peltier elements, it saves cost by reducing complexity of design.

4.5 Thermal Fuse(CP)

Thermal fuses were added in as a mechanical form of safety, see Figure 22. These are designed to blow at a temperature of 73°C. This is far above our defined operating conditions and allows for a safety buffer of peltier control, should software fail. These have been wired in series between the power supply and motor controller as redundancy. Should any issue arise and the temperature rises uncontrollably, all external power fed to the box will be cut.

4.6 Thermistors(TW)

Temperature is sensed using NTC thermistors (EPCOS B57540G1103F000) which have a negative correlation between temperature and resistance. These were chosen due to their size, tolerance and low thermal drift, see Figure 21. As they are small in diameter, measuring 0.8mm across, this allows them to be placed within the thermal interface material to measure the temperature at the surface of the cell and peltier. Their design of glass bead enclosure minimises their drift over time to sub 2% and mitigates for constant calibration at every experiment.

$$R_{th} = \frac{-RV_{th}}{V_{th} - V_{CC}} \quad (3)$$

These were implemented using a Voltage Divider Circuit (VDC), where the voltage dropped across them would be read by the ADC, this voltage would then be able to converted back into the thermistor resistance using a voltage divider equation(3). It is important to note that resistors implemented in the VDC also had a low thermal drift of 50ppm per degree increase in resistance, to minimise error. The resistance can then be interpolated back into temperature either through the β value approximation. Which is a derivation of the Steinhart–Hart equation. The β value approximation has the form:

$$\frac{1}{T} = \frac{1}{T_0} + \frac{1}{\beta} \ln \frac{R}{R_0} \quad (4)$$

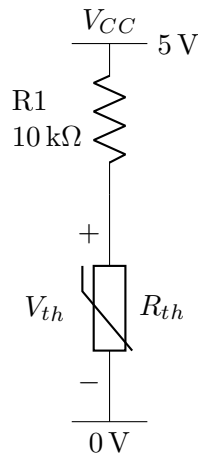


Figure 20: Circuit Diagram of Thermistor Voltage Divider Circuit



Figure 21: Encapsulated Glass Bead NTC Thermistors



Figure 22: Thermal Fuse
Rated to 73°C

Where R_0 is the resistance at temperature T_0 and β is the two point calibration of the thermistor that represents the shape of the curve, it is usually between 25°C and 100°C.

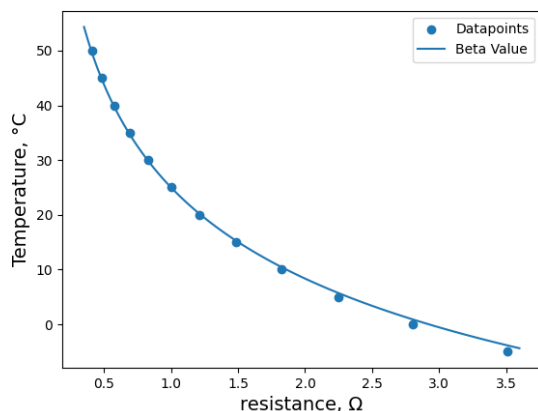


Figure 23: Comparing β Value to the Given Data of Resistance and Temperature.

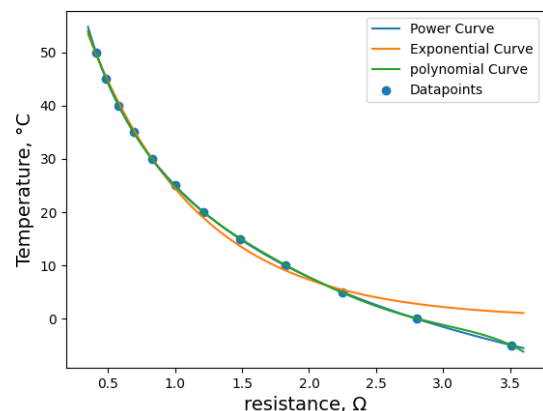


Figure 24: Comparing Different Methods of Interpolating Resistance and Temperature

As shown from 23 there is some error in the reading of temperature especially at low temperatures. For the given resistance at 5 degrees the β value approximation gives a temperature of 5.69 degrees, giving an error of 13.8 %. This error is too large and thus the data points given in the thermistor data sheet will be interpolated. By using 3 different equations as potential fits they can be plotted as shown in 24. An exponential decay, a 5th order polynomial and power law. The exponential curve

does not accurately interpolate by having an R-squared of 0.986, meaning it is not suitable for use of interpolating the temperature. The power curve and the polynomial curve are close with both curves having R-squared values < 0.999. However as the power curve has a lower sum of square errors of 0.0019 compared to the polynomial curves 0.191, it is the desired curve fitting choice. The power curve has the following equation:

$$T = 175.2R_{th}^{-0.1495} - 150.2 \quad (5)$$

4.7 Adafruit ADCs (CP)

The 16 bit Adafruit ADCs (ADS1115) were chosen due to their capability to read 4 single channel inputs. 4 ADC's were integrated into the design to allow for a maximum of 16 single ended inputs. Each ADC communicates via I2C interface with the raspberry pi, allowing for each ADC to communicate on a different channel, their wiring diagram can be seen in Figure 25 [35].

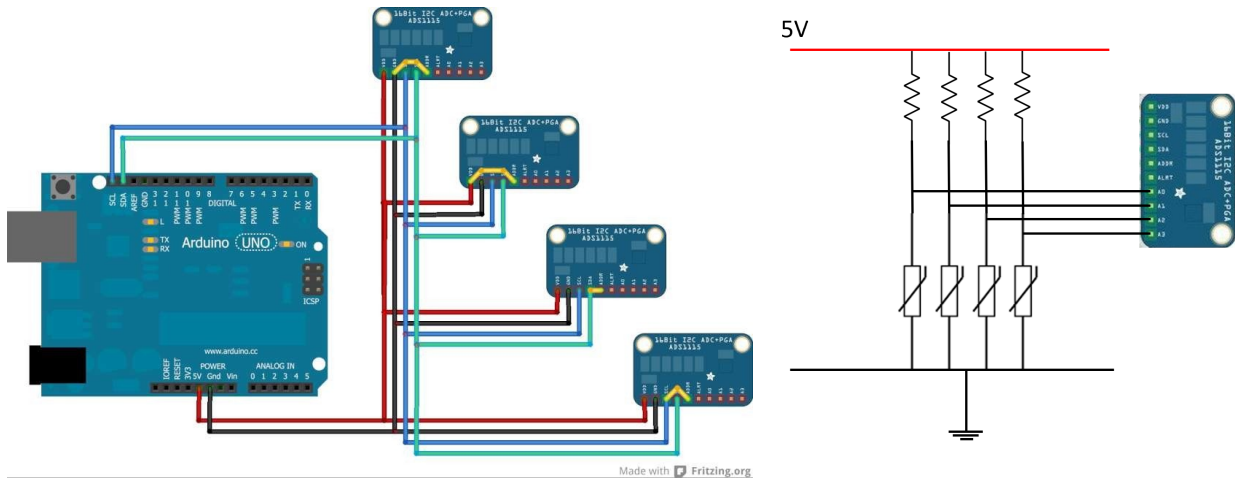


Figure 25: 4 Channel ADC wiring

Figure 26: Voltage Divider Circuit for Thermistor, Read by ADC

For the voltage divider a resistor value had to be found. There are two aims to the voltage divider; first, the divider is desired to be as sensitive as possible; secondly, to draw a safe level of current from the Raspberry Pi GPIO pins.

To have a maximal change, the resistor value should be less than or equal to thermistor impedance. To have a low current draw, the impedance should be as large as possible. The current draw from the GPIO Pins from the Raspberry Pi should not exceed 25mA.

At room temperature, the thermistors impedance sat between 11,800Ω to 12,200Ω. As the thermistors are NTC, their resistances will decrease as temperature rises. For a constant voltage, as Resistance decreases current will rise, as per Ohms Law. Therefore as a safety precaution, a desired current draw from the Raspberry Pi is a degree smaller than rated value when at room temperature resistance. As a current of 2.5mA at 5V is desired at room temperature, a 10,000Ω resistor was chosen for the voltage divider circuit to give a total impedance of 20,000Ω at room temperature.

$$R_T = R_{Thermistor} + R_{Resistor} = \frac{V_{source}}{I_{limit}} \quad (6)$$

$$R_T = \frac{5V}{0.0025A} = 20,000\Omega \quad (7)$$

When reading cell voltage, a dual channel input will be used for greater accuracy. At 5V input, the 16 bit ADC will provide a 76μV resolution for reading cell voltage. For the single channel inputs, a 15

bit signal can be achieved as the first signed bit is not needed. This provides a resolution far greater than required for the thermistors.

4.8 Raspberry Pi (CP)

A Raspberry Pi Model 4B+ is used to control the system. It is the most advanced raspberry pi currently on the market, supporting Ethernet, Bluetooth and WiFi connectivity.

The reason this model was chosen as it allows future implementation of additional technologies such as load banks and live remote feed to a computer via Bluetooth. Furthermore it offers some of the highest processing rate which is desirable for any computationally complex system.

The Pi is able to read, calculate and plot all the desired results. It further saves data to a .txt file to be exported and analysed.

4.9 Water Cooler (CP)

A water cooler aims to keep the surface temperature of one side of the peltiers at a constant. This has two purposes. Firstly, when cooling the block, the waste heat the peltiers are creating can be extracted by the cooling block and the coolant. Secondly, keeping the surface of the peltier at a constant temperature reduces the current that the peltier draws by limiting the temperature difference across the cooler to smaller range.

The coolant pumped through the system is antifreeze, rated to -31°C. Even though the system range is between 5-40°C, it is an over design to allow for a greater range of testing.

5 DESIGN OPTIMISATION

Throughout the build process, issues were discovered and solutions had to be created. The aims of which are to maximise the accuracy of entropy coefficient calculation whilst minimising time taken to carry out the experiment. Minimising fluctuations in voltage and temperature readings were key in obtaining accurate data.

5.1 Filtering and Noise Processing (CP)

Due to the nature of entropy coefficient $\epsilon(SOC)$ changing on the μV level with incremental changes in temperature, extremely high accuracy is desired. Our design included both temperature sensing and voltage measurement methods.

The NTC thermistors resistance changes with temperature in a non-linear way. Each thermistor is minutely different from the other and as such each thermistor follows shifted curves correlating resistance and temperature. When put through our curve fitting function, interpolated from the data sheet, the thermistors showed a vast difference in temperature (Figure 27). Due to the spread, and the thermo-reactive properties within the thermistors, thermistors were all calibrated at the same temperature. Since it is known that water freezes at 0°C, the thermistors were placed in an ice bath and individual resistances read. This allowed their curves to be calibrated to a known temperature. Seen in Figure 28, the thermistors read a temperature difference of $< 0.05C$ between them; this is an increase in one order of magnitude from the uncalibrated difference of $> 0.5C$.

It is evident that the temperature sensing has noise in the system. When isolating one signal, the noise can be seen to be random. However, when opening the scope up to all the signals, the noise repeats in a similar pattern across the full signals. This is indicative of a random error that is present from a source of voltage divider circuitry, see Figure 29 for the source of the voltage. If the thermistors were assumed to be at constant temperature, the total resistance of the circuit would be constant. The rail voltage is also assumed to be a constant value of 5V. However this voltage is supplied from the GPIO pins of the Pi and as such fluctuates. The noise is coming from the voltage source, (Figure 29a). An FFT was carried out upon the signal, this showed no dominant frequency and hence the

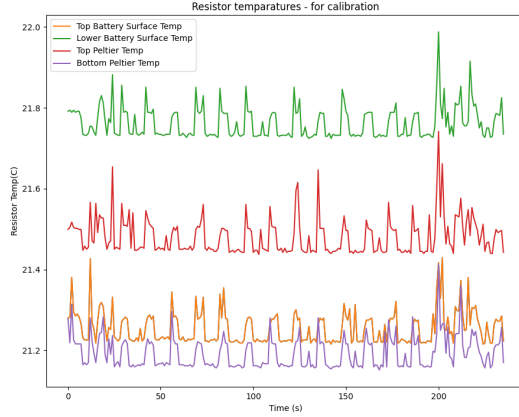


Figure 27: Uncalibrated Thermistor Temperature Readings

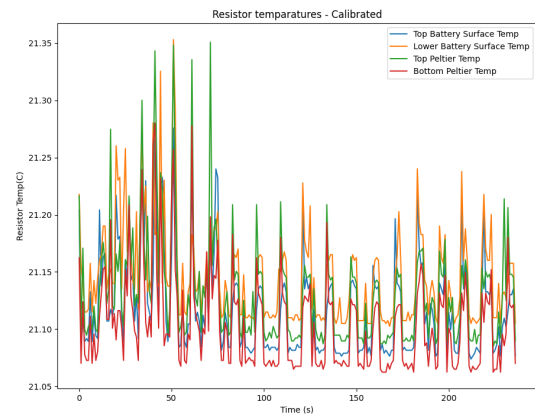
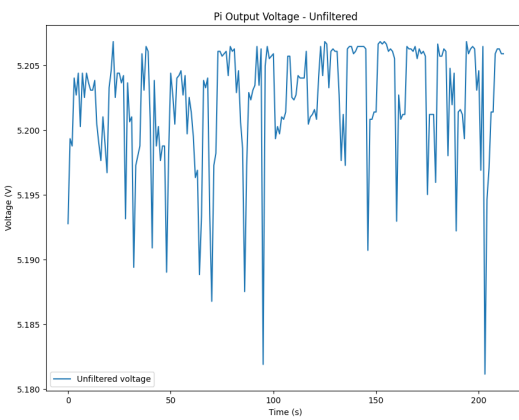
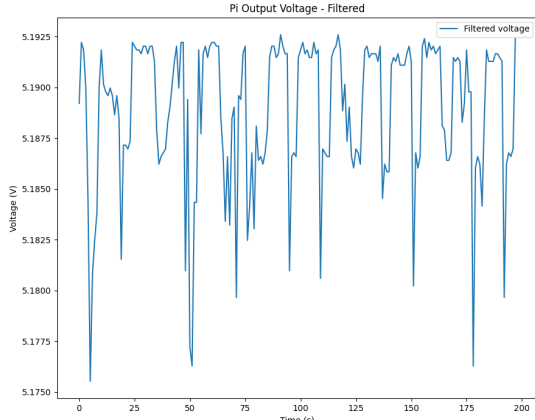


Figure 28: Calibrated Thermistor Values at 0°C

noise was treated as random. Applying a low-pass filter and elimination any high frequency noise was carried out with a voltage regulator circuit comprising of a capacitor in parallel with two inductors, this dropped the voltage range fluctuations from 0.026V to 0.015V (see Figure 29).



(a) Voltage Output Fluctuation from the Pi



(b) Low Pass Filtered Voltage

Figure 29: Voltage Divider Rail Voltage

Due to substantial fluctuations of filtered rail voltage causing a large temperature error, the resistance function was modified. The thermistor temperature function, which previously only measured the thermistor voltage relative the 5V rail, used a separate measurement of the 5V rail to cancel the noise introduced by the 5V rail. Via the dual channel inputs into the ADC, a connection between ground and the +5V rail would provide an accurate reading to 15 bits of accuracy at 6V. This allowed for substantial gains in accuracy as the frequency of large min/max changes in temperature reading reduced (Figure 30). Note that fluctuations still appear due to resistor and thermistor heating as current is passed through them, these are fundamental issues with the components used.

Filtering of the results had been applied to the voltage and errors in the voltage divider circuitry had been analysed. However due to the nature of measuring temperature to a high degree of accuracy, post or real time processing can be implemented. Using a moving mean average, real time processing of data could be used for both cell voltage and block temperature. Sampling size from 5 to 200 data points was chosen to show its effect upon overall fluctuation. The function was applied during the block cooling down in order to see changes in the temperature over time.

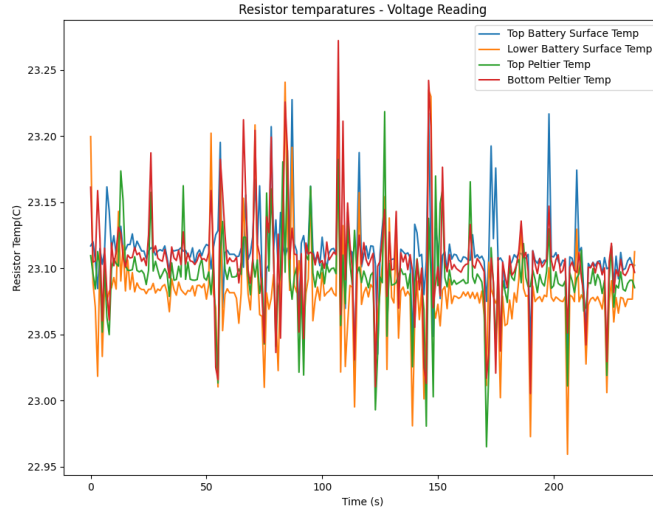


Figure 30: Thermistor Temperatures Calculated by Reading the Voltage from the Pi

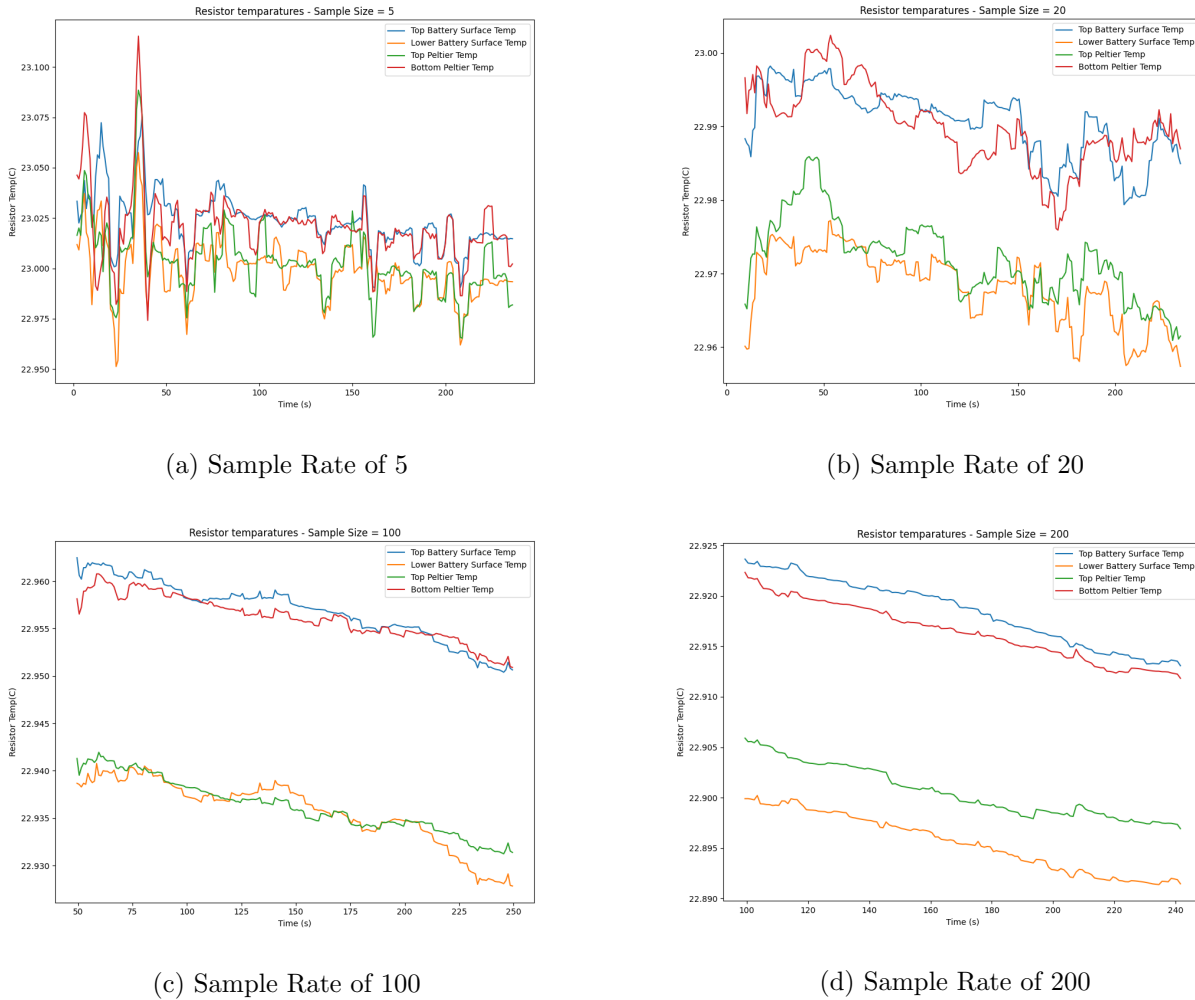


Figure 31: Affect of Moving Average Smoothing Function Sample Rate upon Temperature Reading

Figure 31, shows increasingly more stable outputs of temperature; an effective smoothing function that shows trends more visibly. It also highlights thermistor calibration and the difference of thermistors thermal behavior at different temperatures. Furthermore, as current is passed through thermistors

and resistors, these can self heat and change respective resistance values, affecting overall temperature readings. This is an area of potential development which will be addressed in Section 9.1.

The changes in entropy coefficient are typically very large over a range; the voltage change is typically in the region of mV over steps of $10K$, therefore accuracy on the μV is desired. Modifications and data processing allowed for accuracy to the level of $10\mu V$ and temperature resolution of $0.01^\circ C$ to be obtained.

5.2 Voltage Feedback(TW)

One of the main sources of time for determining the entropy coefficient of a lithium ion cell is the resting time in between temperature steps and allowing the voltage to equalise. This can often be in the order of hours, but it does not have to be. A relaxation time of 5 minutes could be substantial enough [31]. This shorter time needs to be verified by holding the cell's surface at a constant temperature and looking at whether the voltage fluctuates. Through analysis of OCV feedback, the time duration before a temperature step change can be reduced.

5.2.1 Application Of Voltage Feedback on Sample Data(TW)

Assuming that the open circuit voltage follows an exponential profile, it should be possible to predict the outcome of raising the temperature of a cell. By looking at the data from a past experiment run by Dr Hales. It is possible to plot a curve fit of the data. This is done by taking the first n data points and running them through a low pass Butterworth filter twice, this is done to reduce the phase response of the filter to 0 [36]. A curve fitting can then be applied by optimising for values of an exponential decay of the form:

$$y = Ae^{-Bx} + C \quad (8)$$

The values A, B, C from 8 are the values which are being optimised. By repeating this process using $2n$ data points, and by having more data, it will be possible to get a more accurate prediction. By looking at the steady state value of the fitted curve it can be determined when the predictions are not changing. This is done by taking the standard deviation of the past 3 recorded OCV values and determining if deviation has fallen below a certain threshold (0.000002). It can then be assumed that the predictions are not changing and the next temperature step can start. By comparing this early prediction to the full data set allows for verification of the predicted value in terms of how accurate it may be. The exponential predictor will only work when the d^2V_{oc}/dt^2 is negative, this can be achieved by looking at the inflection point of the curve of open circuit voltage.

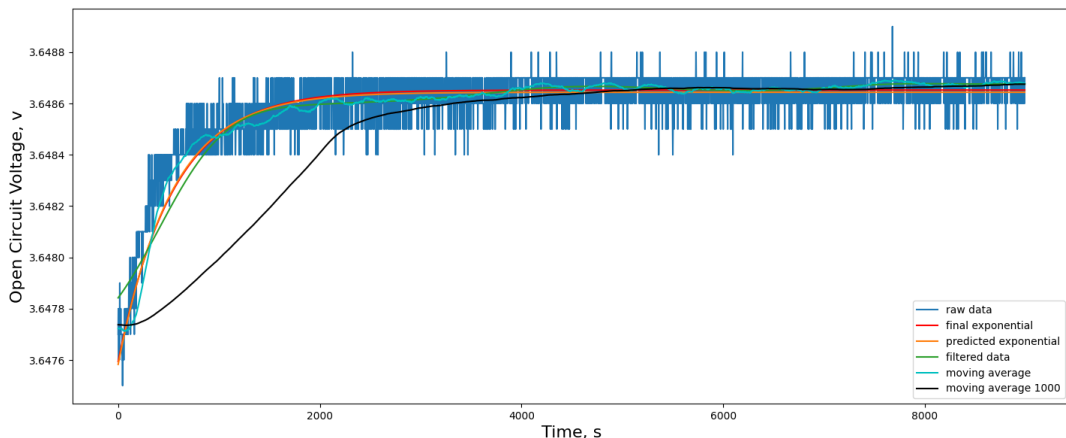


Figure 32: Exponential Predictions of the Final Voltage Equilibrium Point alongside Raw Data, Moving Average and Filtered Data

Figure 32 shows the sample data that has been processed using the method above. The curve fitting function is carried out with $n=400$ and $n=800$ at 3600 seconds into the 8800 second test. This produces two exponential predictions for settling voltage which when compared gives an error of just $8.9\mu V$. This error when compared to the moving average is just $23.7\mu V$ for the full data and $32.4\mu V$ for the prediction at 3600 seconds. However, as the steady state error is lower than the precision of the ADC voltmeter.

The error in this method of voltage prediction can be calculated by comparing the predicted entropy coefficient using the curve fitting versus what the actual entropy coefficient is calculated to be.

| Time of Exponential Prediction (s) | 400 | 800 | 1200 | 1600 | 2000 | 2400 | 2800 | 3200 | 3600 | 4000 | 4400 | 8800 |
|------------------------------------|-------|-------|------|------|------|------|------|------|------|------|------|-------|
| Percentage of Overall Time, (%) | 4.5 | 9.1 | 13.6 | 18.2 | 22.7 | 27.3 | 31.8 | 36.4 | 40.9 | 45.5 | 50.0 | 100.0 |
| Prediction Error, (%) | 37.73 | 11.24 | 8.74 | 7.68 | 6.53 | 4.97 | 4.13 | 3.85 | 3.58 | 3.04 | 2.69 | 2.59 |

Table 2: Curve Fitting Predictions Using Different Amount of Data and their Error

As shown in Table 2 the prediction error reduces as the time increases. There exists a range of points for which the fitting algorithm can produce accurate predictions without taking a significantly long period of time. There is a tradeoff for time taken in the experiment and error value produced. For instance, using just 27% of the overall data gives an error of just 4.97% where doubling the data collected at 50% only reduces the error to 2.69%. In this way, it does not seem viable to continue the experiment on for long periods of time as no substantial improvements are made.

6 IMPLEMENTATION

6.1 Final Design(CP)

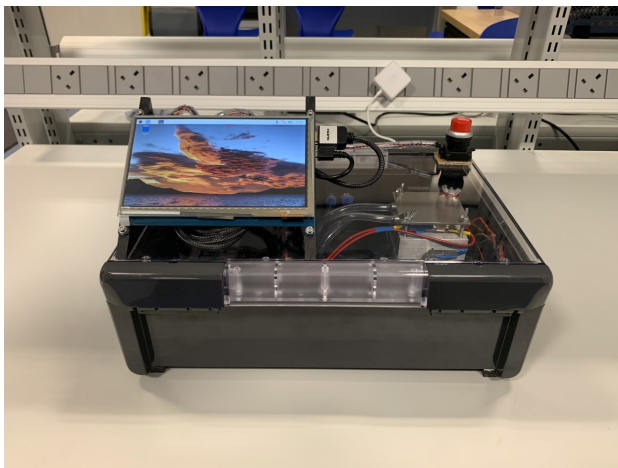
The Final design of the box is shown in Figure 33. Detailed and labeled diagrams are shown in Appendix C.

Figure 33a shows the top face of the box with the screen off to the front LHS, the Pi just behind it and the Kill Switch (KS) to the rear RHS. This was organised in this way, as to allow view of the Li-Cell, coolant connections and thermal fuses, minimising any risk through open display of the actuation unit. The KS is unobstructed to touch, yet it is out of the way of the experiment as minimise accidental depression.

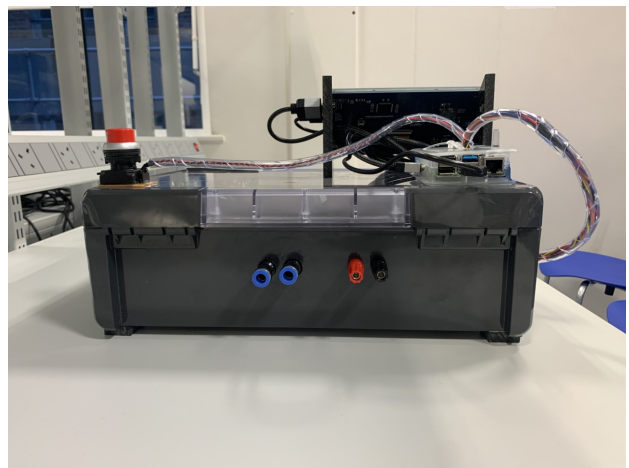
The connections for the coolant and electrical power supply for the motor driver are held at the rear of the box. These allow for push fit, easily attach and detachable connections which are located out of the way from the experiment, allowing the box to be worked on without hazard of cables and pipes getting in the way. Shown in Figure 33b, the Raspberry Pi sits atop the box at the rear, with encased connections coming from it. This allows for hassle-free removal of the Pi if required.

In the lower portion of the box, two sections have been compartmentalised with the electrical compartment being raised off the floor of the box (see Figure 33c). This offers redundant mitigating action in the case of a coolant leak. The sealed compartments should not allow transfer of fluids, yet in the case improbable case that it does, the liquid will pool away from any electronics.

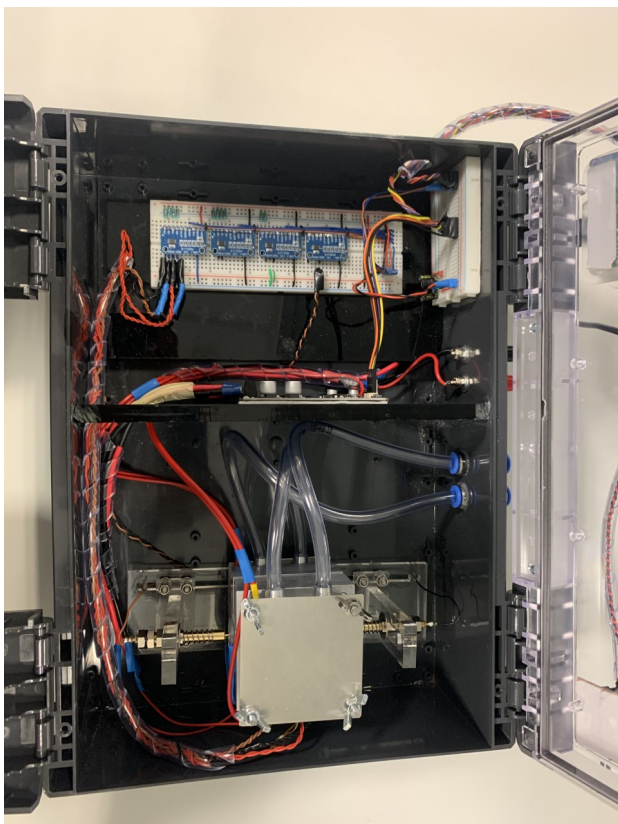
A more detailed view of the the ADC bank, Motor controller and connection board can be seen in Figure 33d. Cables have been routed along the walls as to minimise any disturbance. Further connectors have been fabricated to allow easy plug in of the sensor cables to the correct location on the breadboard. The breadboard has been attached to the rear LHS of the box as to allow easy connections and cable management inside the box. By allowing connections to come in from the Pi via a side hole, easy removal is facilitated. Furthermore the board allows additional connections to be made and box development to occur in the future whilst maintaining a neat and controlled wiring system. This allows for more heating blocks to be implemented within the box with minimal changes



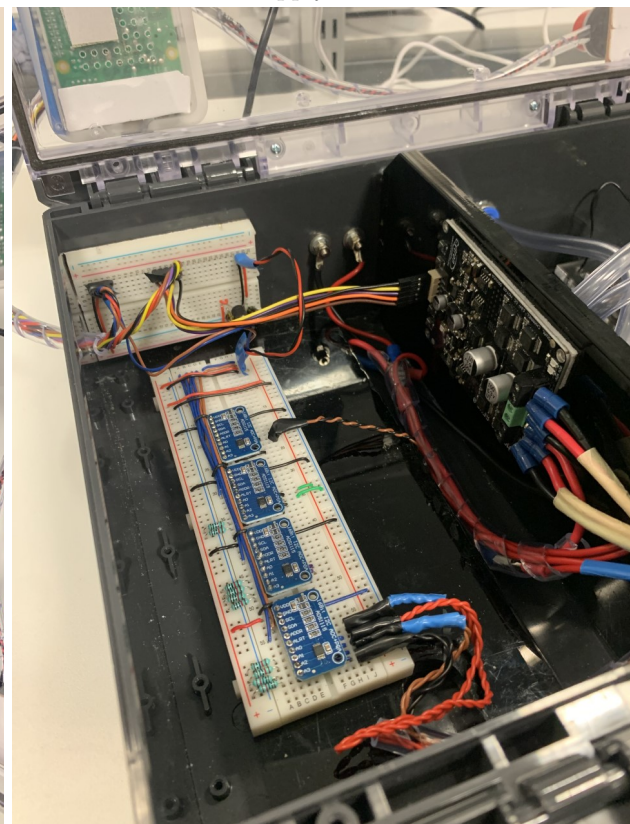
(a) Top of the Box Holds the Screen, Pi and Kill Switch



(b) Rear of the Box Holds the Coolant and Power Supply Connections



(c) Inside the Box Holds the Heating & Cooling Block, ADC Bank and Motor Driver



(d) Electrical Power & Processing Showing the Connections Stemming from the Connection Board

Figure 33: Final Box Design

required. These changes would be made to the code (to activate the new sensors and plot the data) with additional connections plugged into the ADC from the second heating block and voltage probe.

During testing, it was noticed that the Raspberry Pi heated up to a level where it started to affect the speed of calculations. The slowdown was not desired and hence heat sinks were implemented on each of the processors and a further cooling fan was added to the case. This resolved the significant issue of calculation slowdown.

6.2 Controller(CP)

Figure 34 shows an in depth representation of the different systems that make up the closed loop system and the interactions between them.

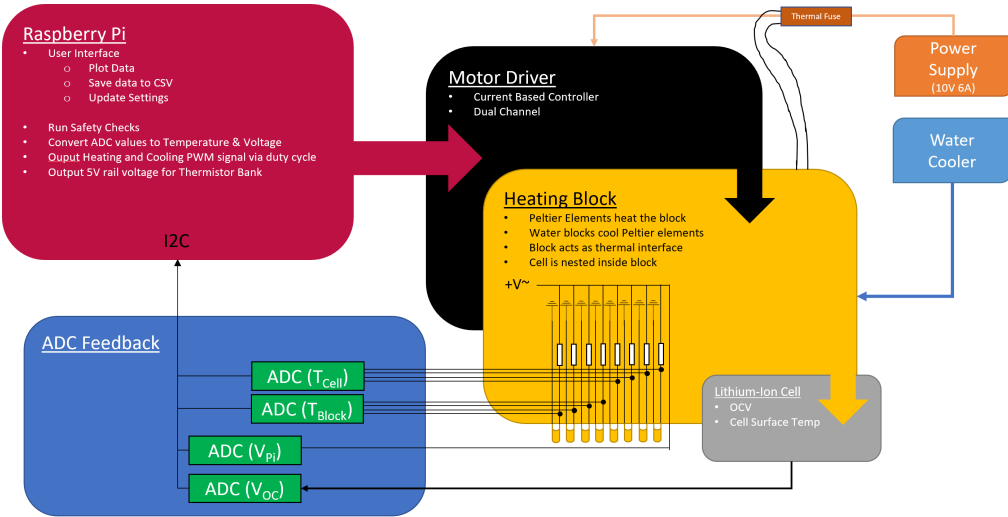


Figure 34: Descriptive Diagram of the Complete Control System

For a desired cell temperature the Pi outputs control signals to the heating elements which applies heating to the cell surface. The temperature of the cell surface is read the thermistors and fed to the ADCs. The feedback from the system comes via the ADC blocks and feeds into the Raspberry Pi.

Figure 35 illustrated the closed loop heating control system with the input as the desired cell temperature with the output of cell surface temperature. The error signal is the difference between the desired cell temperature and the cell surface temperature, shown in Equation 9.

$$error = T_{Desired} - T_{Surface} \quad (9)$$

A PI controller is implemented on the error signal with output fed on to the motor driver. The controller outputs a duty cycle to the motor driver which is saturated at a value of 100%. Further the outputs of the peltier are also limited to a maximum of 50°C for cell safety and 5°C minimum to stop condensation and shorting. These limits add a further point of saturation to the plant output. The gains of the controller K_P and K_I have been set to 25 and 0.1 respectively. Small integral gains were chosen empirically to allow the cell to heat up and stop steady state error without being too great to create substantial integral wind up issues. Proportional gains were set at 25, as for at a temperature difference of 5 degrees, it was desired for the peltiers to heat at a maximum duty cycle and saturate the controller. Though for an error value less than that value, the controller would be able to ramp down its control and allow the cell to safely reach its desired thermal state. These gains are set as to achieve a suitable thermal rise time without posing a risk to safety.

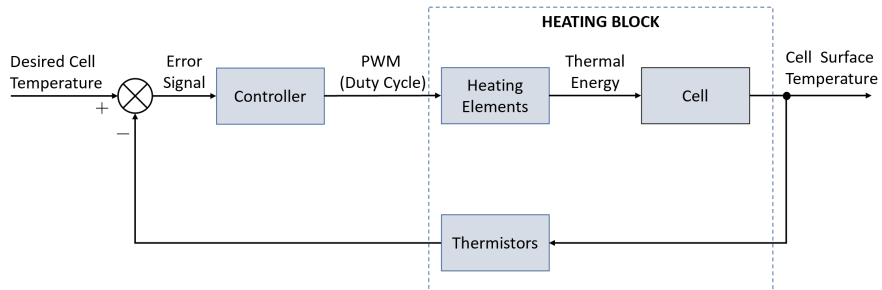


Figure 35: Diagram of the Closed Loop Control of Thermal Actuation

6.3 Overview of a Test Cycle(CP)

The aims of the test cycle is to thermally cycle the cell. This process is carried out via the Display and User Interface. The use of the User Interface is detailed in the User Guide section.

The experiment is carried out over a set temperature range with the temperature steps or nodes being pre defined. The control system individually steps to these temperatures and maintains the cell at the desired step temperature. Once reached, the OCV is allowed to stabilise. Determination of stability is decided by the voltage feedback control system and will allow the experiment to progress to the next step once a predefined value of standard deviation or minimum voltage fluctuation value has been obtained. This process repeats, stepping each time until the full range of temperatures has been explored.

The output of the experiment is the entropy coefficient values for each temperature step. This data is output to a CSV file which can be read from the display or loaded onto a USB memory stick via the Pi.

7 RESULTS AND ANALYSIS

7.1 Thermal Rise and Fall Time(TG)

To determine the effect on thermal performance of the cooling fluid temperature, two experiments were conducted over the same temperature steps. Temperature was stepped from 20-10-20-40-10 to provide a few different heating and cooling scenarios. Figure 36 shows the recorded temperatures for when a coolant of 10 degrees and 20 degrees were used respectively.

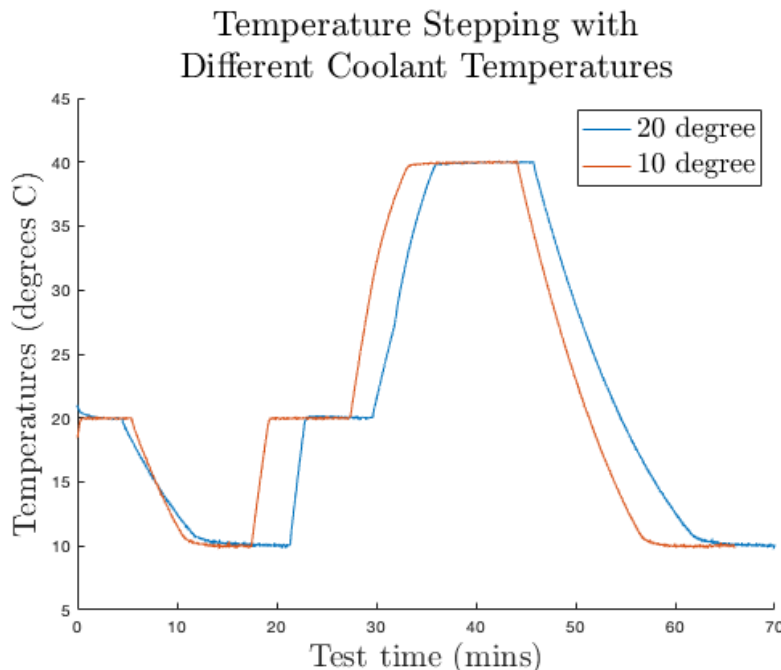


Figure 36: Comparing Temperature Step Times for Coolant at 10°C and 20°C

Cooling/heating performance is measured by Top cell temperature as this is of critical importance. The time taken for temperature steps was interpolated from Figure 36 and is presented in Table 3. Here total experiment time is not an indication of heating/cooling time as the time between temperature steps was not controlled. Instead the gradient of the line can be used as a visual indication of the heating/cooling performance. For example for the initial step of 20-10 degrees the orange line (10 degree coolant) is clearly steeper than the blue line (20 degree coolant). A 10 degree rise time can be carried out by the block in 2 minutes, when coolant is circulating at 10 degrees.

Table 3 shows the results. Delta (s) is the time taken for a temperature step, and 20 degree coolant takes longer for cooling steps when compared to the 10 degree coolant. The average percentage reduction in step time is 22% for cooling steps whilst for heating steps the data is inconclusive. The 22% improvement for cooling steps is because the peltiers are able to achieve a lower temperature more quickly on the block side, as the temperature difference required across the Peltier is less when the cooling block is colder.

| Temp Step | Heating / Cooling | Temp Change | 20 Coolant Temp | | | 10 Coolant Temp | | | % Time reduction by using 10 deg | Average |
|-----------|-------------------|-------------|-----------------|----------|-----------|-----------------|----------|-----------|----------------------------------|---------|
| | | | Start (s) | Stop (s) | Delta (s) | Start (s) | Stop (s) | Delta (s) | | |
| 20 to 10 | Cooling | 10° | 4.48 | 11.89 | 7.41 | 5.42 | 10.87 | 5.46 | 26.37% | 24.28% |
| 10 to 20 | Heating | 10° | 21.31 | 23.03 | 1.72 | 17.44 | 19.36 | 1.92 | -12.08% | -4.14% |
| 20 to 40 | Heating | 20° | 29.54 | 37.01 | 7.47 | 27.41 | 34.60 | 7.18 | 3.81% | |
| 40 to 10 | Cooling | 30° | 45.73 | 62.85 | 17.12 | 44.13 | 57.45 | 13.32 | 22.19% | |

Table 3: Thermal Performance with Coolant Temperature

7.2 Voltage Settling Time Determination(TW)

Once a temperature step has been achieved it is necessary for the open circuit voltage to settle. Typically in climate chambers this is done by waiting a long amount of time (in the order of hours), Osswald et al. determines it is possible to wait for 5 minutes after the internal temperature of the cell has reached equilibrium. This was done by observing the internal temperature of the cell and waiting for that to reach equilibrium, meaning that it is assuming that the whole cell is in thermal equilibrium and that the cells open circuit voltage is also in equilibrium. To get a more robust result of determining when the open circuit voltage is in equilibrium the standard deviation of previous values can be taken to measure when the voltage is changing.

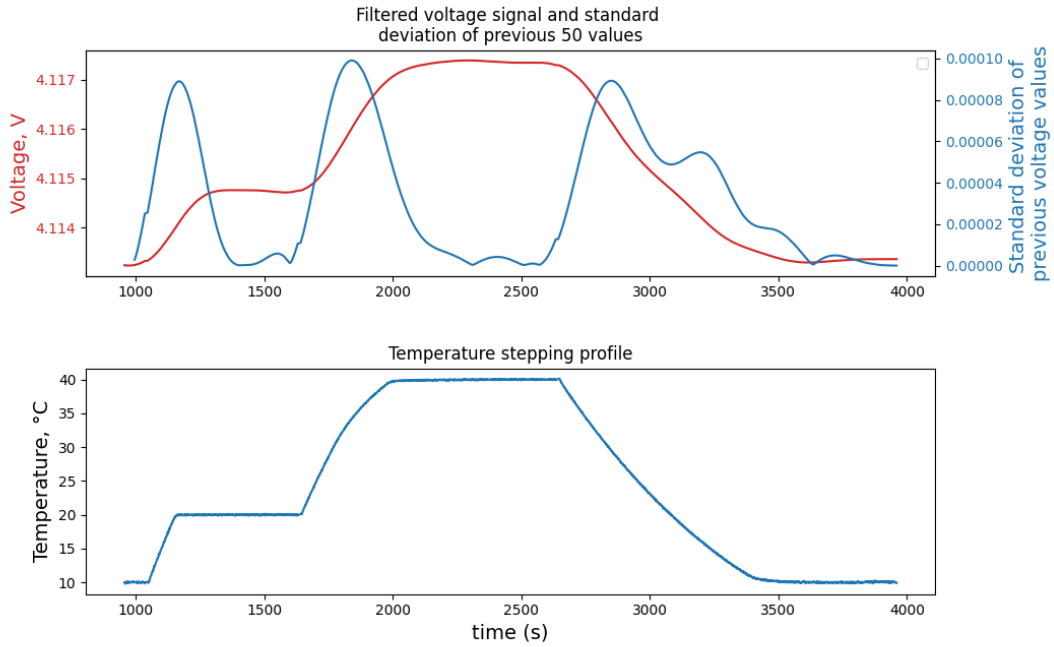


Figure 37: Filtered Cell OCV Profile and the Respective Standard Deviation Values over Temperature Stepping Profile

Figure 37 shows the voltage that has been passed through a low pass filter, a standard deviation of the past 50 values was then taken to determine when the voltage is changing. It can be seen in the period of 1000 to 1300 seconds that the voltage is rising due to a temperature step between 10 and 20°C, and the standard deviation of previous values is high. In the period of 1400 to 1600 seconds the

standard deviation of previous values is smaller than 1×10^{-5} . This same pattern can be seen with the other temperature rises.

The application of this method shows that if a tolerance level was set for the standard deviation, for example 1×10^{-5} and the standard deviation stays below this for an amount of time, for example 150 second. This can be assumed to be when the voltage has leveled off and is no longer changing. So the voltage can be measured, the entropy coefficient calculated and the next temperature step can be started.

For the temperature step from 10°C and 20°C the temperature step occurs between 1060 seconds to 1210 seconds, but using the method in Osswald et al. the voltage would be measured 5 minutes after this. But from looking at the standard deviation of previous values falling below the threshold of 1×10^{-5} and staying below that for 150 seconds, the standard deviation falls below the threshold at 1330 seconds giving a settling time of 4.5 minutes. Using the method in Osswald et al. would take until 1510 seconds until the voltage has settled giving. This method gives similar results in the settling time of open circuit voltage that agree with both the waiting time in Osswald et al. and that of the thermal settling time modeled in Section 2.

7.3 Time Efficient Accuracy of Entropy Coefficient Determination (TG/TW/CP)

In this section results of entropy coefficient measurement are presented and discussed. The specific cell being tested is the LG M50 21700 at SOC of 94% and 84%. Two temperature step cycles are presented below in Fig 38. Both were completed in the same day only minutes after one another, with no charging or discharging of the cell between tests. The voltage reading for both graphs represents a moving average of the measured voltage, this is discussed in Section 6.1.

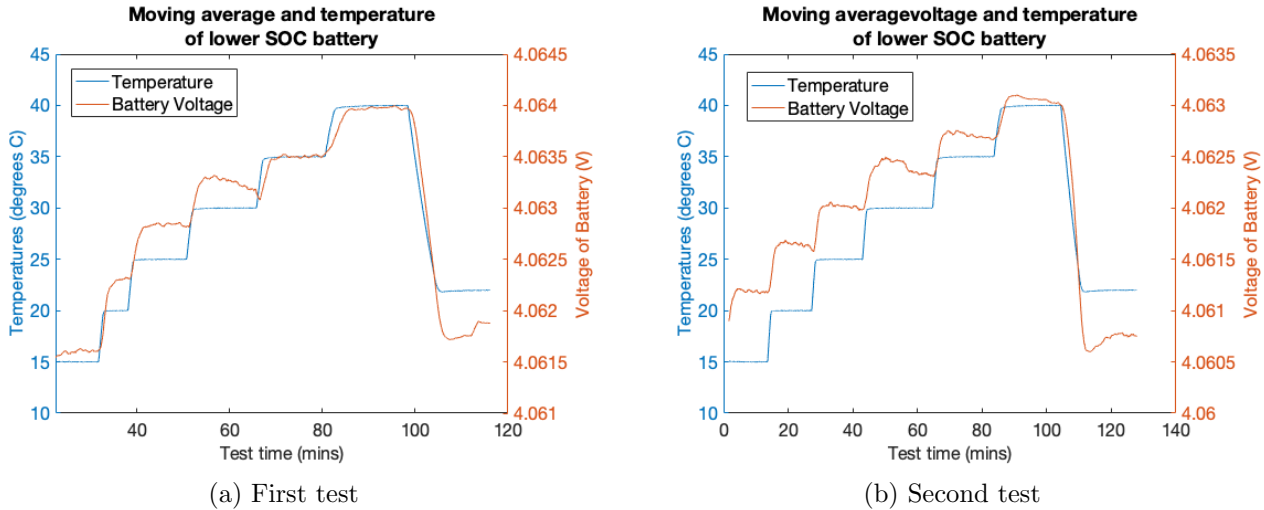


Figure 38: Tests on 84% SOC Cell with Temperature Steps of 15, 20, 25, 30, 35, 40, 22°C

Both tests 38a and 38b are demonstrations of the effectiveness of the cooling/heating ability of the device as the temperature stepping takes minimal time compared to voltage equalisation. For the majority of steps over 10 minutes is waited at each step whilst the voltage equalises which is thought to be more than enough to obtain an accurate result [31]. Should a shorter time at each step be taken it is estimated that a full test similar to the industrial standard [26,27] of 5°C temperature increments from 5-40°C could be completed in one hour, which is far below the industry standard of 15-24 hours.

The entropy coefficient measurements for 38a and 38b are below tabulated in Table 5 and the results are displayed in Fig 39a. Table 5 shows the spread of results for the first and second tests and a combined spread. The precision of the first test is clearly much worse than the second however this is largely due to the two results for 15°C to 20°C and 20°C to 25°C . This is likely due to the shortened temperature step in 38a which can be seen at around 30-40s. The voltage after this step did not have time to equalise and would have effected both the results previously mentioned. If these results

| Experiment (SOC) | Min-Max Range ($\mu V/K$) | Interquartile Range ($\mu V/K$) |
|------------------|-----------------------------|-----------------------------------|
| 84% (a) | 72 | 50 |
| 84% (b) | 22 | 15 |
| 94% (a) | 19 | 11 |
| 94% (b) | 25 | 20 |

Table 4: Entropy Coefficient Measurement Ranges for 84% and 94% SOC

| Temperature Step (s) | a) | b) |
|----------------------|----------|----------|
| 15 to 20 | 1.36E-04 | 9.12E-05 |
| 20 to 25 | 1.04E-04 | 7.95E-05 |
| 25 to 30 | 7.69E-05 | 6.93E-05 |
| 30 to 35 | 6.43E-05 | 7.31E-05 |
| 35 to 40 | 9.24E-05 | 7.43E-05 |

Table 5: Entropy Coefficient Measurements for Cell at 84% SOC

are neglected then the combined spread is visually quite similar to the spread of the second test. Although there are not enough data points to fully assess the accuracy, the available data points suggest repeatability in the experiment.

Another experiment was carried out on the same cell at a higher SOC of 94%. This was done to validate the setup, where, due to this higher SOC it is expected that the entropy coefficient will be higher than when the cell is at a lower SOC. Comparing the results from Figures 39b and 39a show this is true.

Comparing the measurements of entropy coefficient from the experiments allows the accuracy of the design to be quantified. Experiment 84(a) (Figure 39a) can be declared as anomalous when compared to the other experiments with a range quadruple that of the others. The further experiments show at most a min-max range of $25\mu V/K$ and an interquartile range of $20\mu V/K$, see Table 4. Allowing for slight fluctuations due to noise, a conservative resolution of $30\mu V/K$ can be consistently determined by the apparatus.

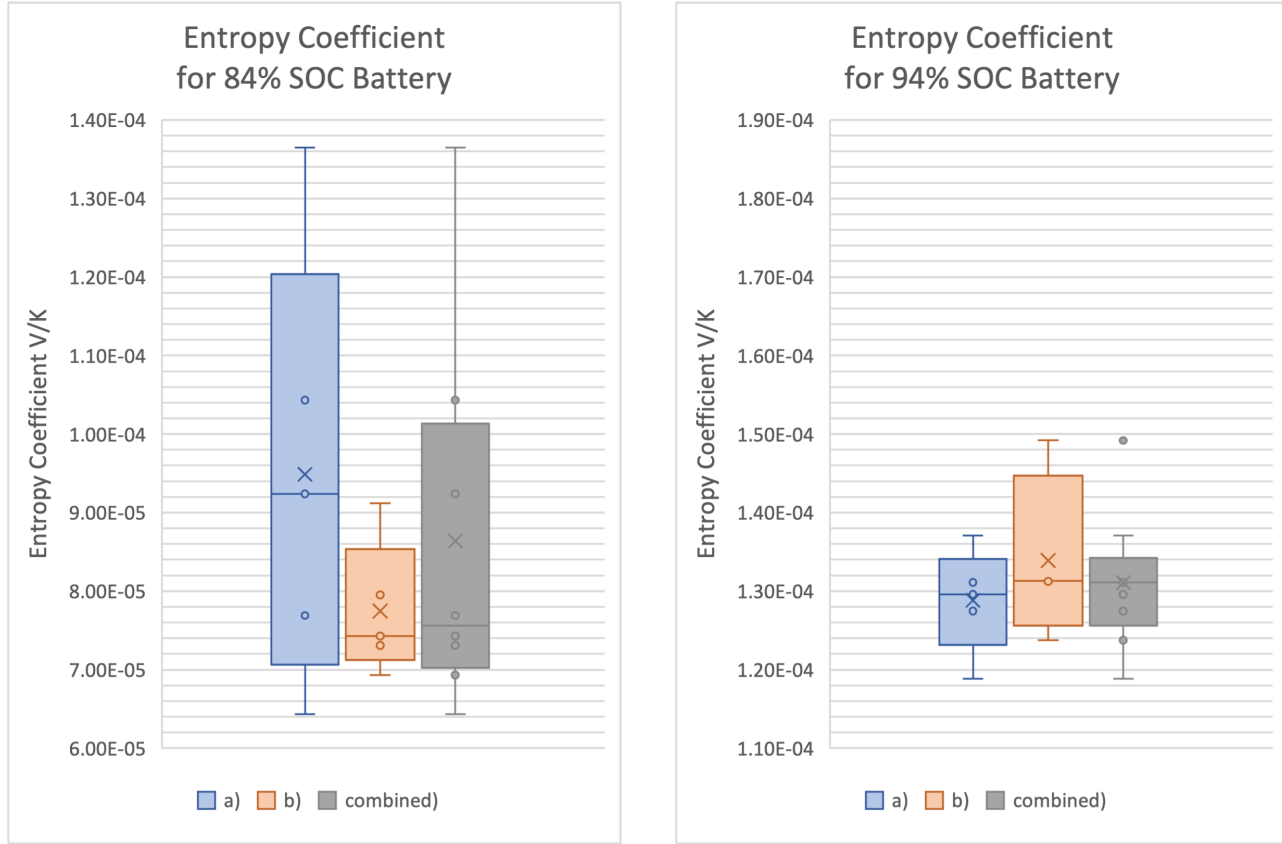


Figure 39: Mean and Spread of Entropy Coefficient Measurements Over 4 Temperature Steps.

8 DISCUSSION

8.1 Design Comparison(CP)

The design proposed offers to carry out entropy coefficient experiments in a reduced time frame. It builds off the idea of potentiometric testing, however voltage feedback allows for a faster step time to be obtained and hence overall speed is much faster. Though there is lack of cell cycling SOC within the experiment, a temperature profile can take between 5-30 minutes which is still significantly greater than the industry standard.

Comparing the our heating method to literature and modelling shows its validity. Estimations of thermal settling time at around 5 minutes was quoted from literature . The heating block achieved these heating and cooling in less than half of that with minimal variance which only goes to prove the concept of heating via solid thermal interface is better than the climate chamber.

Methods proposed also suggested cell temperature regulation via fluid. Though this method also is able to heat the cell homogeneously it is an over design. Our design is able to reach desired temperatures at a faster rate than the fluid in Osswald et al. This is mainly due to the specific heat capacities being greater than that of our thermal block and further the block offering better conductive heating. Furthermore the simple design offers a cheaper alternative to the current fluid design. An important design choice to note is that our design offers a clean solution where easily spillable liquids are contained. A possible design choice for the design could be to remove the water cooling in replace of a heat sink if fluids should not be used.

Focusing on not just the experiment but the design approach, the design as a whole offers large functionality. Through presetting of variables such as temperature steps (standard deviation, OCV feedback, range etc) and the ability to change and tweak all settings that affect the cells entropic heating allows for greatest testing and investigation into a cells characteristics. Combined with the ease of use of the design to carry out experiments is a positive note. Furthermore, design choices have been made to ensure future developments upon the prototype can be made and implemented with ease. This allows for greater use of this tool and further improvements in the field to be made.

8.2 Design Limitations(CP/TW)

The limitations of the system design can be split up into sections as to better understand the factors at play. These consist of effects upon:

- System Control
- Time-frame of Experiment
- Accuracy of Data
- Reliability of Data

Unable to complete a full entropy coefficient profile of the cell is due to the lack of a cell-cycler. In that the SOC is not able to be varied during the experiment and hence a complete profile of the cell cannot be obtained without external equipment. This lack can be argued to also increase the time of a full experiment as SOC, through further OCV feedback, cannot be monitored within the experiment. The control system is also unable to interface directly with the cooling cycler, consequently the efficiency in both time and energy of the experiment can suffer over the full temperature cycle.

Time-frame of the experiment is mainly affected by the temperature and mainly temperature changes of the block. Primarily lack of power available to heat the block caused a reduction in the rise time of the peltier elements and hence the cell. A sharper increase in peltier temperature results in a faster temperature rise of the cell surface. Being able to respond to a demand temperature hastily allows for a shorter thermal equilibrium time, thus a faster electrochemical equilibrium as the OCV of the cell equalises. Overall this results in a shorter entropy coefficient acquisition time. The main limiting factor of the thermal rise time has been the bench-top power supply used (NGE - 100) . The power supplies have a maximum output power of 33.6 W per channel limiting the power supplied to the motor controller and the peltiers, which are in turn also limited by their power output.

A further limitation upon time frame presents itself within the Raspberry Pi. As the Raspberry Pi heats up over time, the time taken to carry out each calculation and tick gradually starts to increase. Though implementation of cooling fans and heat sinks are in place, inefficient heat dissipation only sees to slow the experiment.

The size of the block limits time-frame of the experiment through its thermal capacitance. By offering a more stable temperature through minimising convection and maximising conduction, the cell can be held at a homogeneous surface temperature. However, time taken to heat and cool the cell increase as its overall heat capacity increase. This is further opposed by lack of insulation and an increase in heat dissipation via convection of the block surface.

There was a small thermal gradient in the block measured using the holes throughout the block, this gradient became increasingly smaller the longer the experiment ran, the thermal gradient between the centre of the block and the outside edge was less than 0.1°C which provides confidence that the cell was heating homogeneously. Improvements could be made by insulating the heating block on the open sides, this would also have an added advantage of potentially reducing the thermal rise time due to heat lost to the surroundings and a reduction power consumption when in steady state.

Higher precision of voltage measurement would allow for more accurate calculation of cell entropy coefficient. Resolution is limited by the 16bit ADC, where a higher bit ADC would be more suitable in its place. Voltage fluctuations and noise, mainly due to breadboard connections further hampered accuracy of OCV due to rails acting like antennae [37]. Due to the noise and precision of measuring OCV the method of curve fitting shown in Section 5.2 could not be applied to the experiments conducted, this is due to the noise causing the shape of the rise of OCV to not follow an exponential curve. But the code for making the predictions was implemented to be able to run in real time and when the difference in curves fell below a threshold the next temperature step would start.

Temperature of the cell measured through thermistors had a high enough resolution, however the individual temperature curve for each thermistor showed drift. Though only minimal when calibrated, the presence of drift adds inaccuracies to the data set collected.

Reliability of data can be improved through testing of multiple cells. Lack of availability of numerous samples inhibited true realisation of the apparatus's potential and offered lesser reliability when comparing produced data sets to published.

9 CONCLUSION (CP)

The design of the apparatus has been carefully considered to produce accurate and precise data in a time efficient manner whilst maintaining safety for the user.

Entropy coefficient determination of the LG M50 21700 cell was able to be carried out, with repeatable and accurate data producing consistent results. A determined entropy coefficient range of less than $30\mu\text{V}/\text{K}$ was able to be measured, far exceeding original expectations and design specification of $1\text{mV}/\text{K}$. The time required to heat the cell and measure the entropy coefficient was 7 minutes for a 10 degree temperature step. A 2 minute heating time and 5 minute voltage settling time. This method offers a 97% reduction in the current industry standard time taken to carry out the same process.

Measurement of the cell voltage was able to achieve a resolution of $180\mu\text{V}$. Though this value is higher than required by the design specification, it still enabled high enough entropy coefficient measurement accuracy to meet specifications. The lower voltage measurement accuracy was mainly due to fluctuations in OCV and less accurate than desired ADCs. The OCV feedback showed proof of concept through its application to sample voltage and temperature data. It produced accurate predictions of the voltage equilibrium point to less than 5% error, in less than one third of the total experiment time. When OCV feedback was applied to the apparatus, the large amount of noise within the system prevented the feedback system from working as intended. Issues with noise have been identified and solutions realised, this is covered in greater dept in Section 9.1.

Temperature actuation and measurement proved successful on both fronts. Firstly, a resolution of

$1mK$ can be achieved with the existing ADC and thermistors setup. These values are more accurate than initial specification requirements even through the noise and other issues with the design, which have been identified in greater depth in Section 9.1. Secondly, the thermal actuation design is successful in heating the cell homogeneously in a period of time that is far smaller than that of the industry standard. Further improvements of the time efficient heating of the block come from setting the coolant temperature to 10°C for the duration of the thermal cycle. On the other hand, climate chambers are not time efficient in heating up a cell when compared to a thermal interface conduction method. Therefore the method of thermal actuation within this design exists as a proof of concept, offering reliable, fast and homogeneous heating to cells when compared to climate chambers.

Overall the apparatus as a whole proved to provide compact and triple safely redundant design. Ease of use was achieved through the GUI as experiments could be controlled, displayed and variables changed within the system. A user guide has been created with important instructions laid out within the GUI, this can be seen in Appendix B. The design offers a viable testing method of thermal actuation and OCV feedback through repeatable, consistent and precise data. However, due to lack of readily accessible sample data of the LG M50 cell no validation of entropy coefficient measurements could be made.

With reference to the aims and objectives laid out in Section 1.6 the apparatus exceeds thermal actuation and temperature measurement specification however falls short of voltage measurement accuracy specification. Despite this the entropy coefficient measured falls under the specified accuracy. Furthermore, the time taken for a temperature step was greatly reduced when compared to the specification. The final produced design offers viable methods to measure the entropy coefficient of a cell faster than the industrial standard.

9.1 Areas of Future Research & Development(CP)

Throughout the building testing phases of the empirical process, key areas of limitation and improvement were identified. They can be categorized into two key areas; development of the physical test instruments and areas of further research and testing. Investigating and implementing change in these areas will allow for more accurate and faster testing with a better holistic understanding of the behavioural characteristics of entropy coefficient and the factors of the cell which affect it.

Increasing the accuracy of the experimental apparatus can be developed in both the voltage and temperature sides of the control system. For hardware, a higher 20bit ADC has determined to provide suitable resolution for testing, detecting a step change of $4.7\mu\text{V}$. Further fluctuations of voltage noise can be eliminated through fabrication of a integrated PCB for the ADC's and their connection as opposed to breadboards which are currently used.

For temperature detection, improvements in accuracy can be made through software. Thermistor calibration through the experiment can allow for more accurate compensation for individual thermistor and resistor drift in the VDC, resulting in a more accurate thermal reading hence a more accurate entropy coefficient determination. Further improvements in rail voltage stabilisation and filtering will only see for more stable readings and a significant reduction in noise. Hardware improvements can also come from block insulation to minimise convection and hold a more stable block temperature. This furthers investigation into the effect of tab convection of the cell affecting cell temperature homogeneity and as a consequence, entropy coefficient calculation.

Upgrades to the apparatus can come from both hardware and software. Reliability of data and greater testing capacity can be increased through additional cell blocks being added. Space has been left within ADC channels to allow for such additions to be made. Moreover, to increase the ability of the apparatus to carry out a full entropy profile of a cell, a cell cycler should be integrated into the design. This can simply be done by interfacing the OCV feedback with the controller to detect changes in SOC.

Principal to the implementation of a cell cycler is the understanding of electrochemical equilibrium. As the cell SOC changes so does the OCV, hence the same OCV feedback could theoretically be used

to detect electro-chemical equilibrium as well as thermo-electrical equilibrium.

Software of the voltage OCV curve fitting requires investigation of greater depth. Though proof of concept shows voltage stabilizing, lack of high accuracy OCV measurement obstructed greater testing to be carried out. Investigation into varying values of standard deviation and/or average OCV values which flag for a temperature step change need to be better understood. Specifically, the way in which these values affect measurement accuracy and experiment duration and the trade off between them. More specifically, this allows for preset tests to be defined, one for a faster experiment of lesser accuracy, or a slower more precise test cycle.

ACKNOWLEDGEMENTS

We would like to express our gratitude to our exceptional supervisor Dr. Alastair Hales who has provided unwavering support and guidance thought this research project. Thank you Gavin White for your time engaging and sharing ideas of his existing and exciting projects on peltier control modules. Thank you James Filbin and Terry Godsmark for helping us manufacture the prototype. Rich Walker, Amy Bland, and the rest of technical services for helping us with any questions that we had.

REFERENCES

- [1] R. T. Doucette and M. D. McCulloch, "A comparison of high-speed flywheels, batteries, and ultracapacitors on the bases of cost and fuel economy as the energy storage system in a fuel cell based hybrid electric vehicle," *Journal of Power Sources*, vol. 196, no. 3, pp. 1163–1170, 2011. [Online]. Available: <https://www.sciencedirect.com/science/article/pii/S0378775310015855>
- [2] IEA, "Energy technology perspectives," 2017. [Online]. Available: <https://www.iea.org/reports/energy-technology-perspectives-2017>
- [3] G. Zubi, R. Dufo-López, M. Carvalho, and G. Pasaoglu, "The lithium-ion battery: State of the art and future perspectives," *Renewable and Sustainable Energy Reviews*, vol. 89, pp. 292–308, 2018. [Online]. Available: <https://www.sciencedirect.com/science/article/pii/S1364032118300728>
- [4] L. Chen, X. Fan, E. Hu, X. Ji, J. Chen, S. Hou, T. Deng, J. Li, D. Su, X. Yang, and C. Wang, "Achieving high energy density through increasing the output voltage: A highly reversible 5.3 v battery," *Chem*, vol. 5, no. 4, pp. 896–912, 2019. [Online]. Available: <https://www.sciencedirect.com/science/article/pii/S2451929419300385>
- [5] M. Lenz, T. Hoehl, L. Zanger, and S. Pischinger, "Approach to determine the entropy coefficient of a battery by numerical optimization," *Journal of Power Sources*, vol. 480, p. 228841, 2020. [Online]. Available: <https://www.sciencedirect.com/science/article/pii/S0378775320311459>
- [6] S. J. Gerssen-Gondelach and A. P. Faaij, "Performance of batteries for electric vehicles on short and longer term," *Journal of Power Sources*, vol. 212, pp. 111–129, 2012. [Online]. Available: <https://www.sciencedirect.com/science/article/pii/S0378775312007069>
- [7] L. Lu, X. Han, J. Li, J. Hua, and M. Ouyang, "A review on the key issues for lithium-ion battery management in electric vehicles," *Journal of Power Sources*, vol. 226, pp. 272–288, 2013. [Online]. Available: <https://www.sciencedirect.com/science/article/pii/S0378775312016163>
- [8] J. B. Quinn, T. Waldmann, K. Richter, M. Kasper, and M. Wohlfahrt-Mehrens, "Energy density of cylindrical li-ion cells: A comparison of commercial 18650 to the 21700 cells," *Journal of The Electrochemical Society*, vol. 165, no. 14, pp. A3284–A3291, 2018. [Online]. Available: <https://doi.org/10.1149/2.0281814jes>
- [9] A. Manthiram, "An outlook on lithium ion battery technology," *ACS Central Science*, vol. 3, no. 10, pp. 1063–1069, 2017, pMID: 29104922. [Online]. Available: <https://doi.org/10.1021/acscentsci.7b00288>
- [10] H. Zhang, Y. Yang, D. Ren, L. Wang, and X. He, "Graphite as anode materials: Fundamental mechanism, recent progress and advances," *Energy Storage Materials*, vol. 36, pp. 147–170, 2021. [Online]. Available: <https://www.sciencedirect.com/science/article/pii/S2405829720304906>
- [11] B. Chapman, "How does a lithium-ion battery work?" 2019. [Online]. Available: <https://letstalkscience.ca/educational-resources/stem-in-context/how-does-a-lithium-ion-battery-work>
- [12] N. Nitta, F. Wu, J. T. Lee, and G. Yushin, "Li-ion battery materials: present and future," *Materials Today*, vol. 18, no. 5, pp. 252–264, 2015. [Online]. Available: <https://www.sciencedirect.com/science/article/pii/S1369702114004118>
- [13] R. D. Deshpande and D. M. Bernardi, "Modeling solid-electrolyte interphase (SEI) fracture: Coupled mechanical/chemical degradation of the lithium ion battery," *Journal of The Electrochemical Society*, vol. 164, no. 2, pp. A461–A474, 2017. [Online]. Available: <https://doi.org/10.1149/2.0841702jes>
- [14] K. E. Thomas and J. Newman, "Thermal modeling of porous insertion electrodes," *Journal of the Electrochemical Society*, vol. 150, no. 2, p. A176, 2003.
- [15] C. Forgez, D. Vinh Do, G. Friedrich, M. Morcrette, and C. Delacourt, "Thermal modeling of a cylindrical lifepo₄/graphite lithium-ion battery," *Journal of Power Sources*, vol. 195, no. 9, pp. 2961–2968, 2010. [Online]. Available: <https://www.sciencedirect.com/science/article/pii/S037877530901982X>
- [16] D. Bernardi, E. Pawlikowski, and J. Newman, "A general energy balance for battery systems," *Journal of The Electrochemical Society*, vol. 132, no. 1, pp. 5–12, jan 1985. [Online]. Available: <https://doi.org/10.1149/1.2113792>
- [17] S. S. Madani, E. Schaltz, and S. Knudsen Kær, "An experimental analysis of entropic coefficient of a lithium titanate oxide battery," *Energies*, vol. 12, no. 14, 2019. [Online]. Available: <https://www.mdpi.com/1996-1073/12/14/2685>
- [18] T. K.E., B. C., and N. J., "Measurement of the entropy of reaction as a function of state of charge in doped and undoped lithium manganese oxide," *Journal of the Electrochemical Society*, vol. 148, no. 6, p. A570–A575, 2001, cited by: 105. [Online]. Available: <https://www.scopus.com/inward/record.uri?eid=2-s2.0-0001733612&doi=10.1149/\%2f1.1369365&partnerID=40&md5=980008e3bce8170fc80e2230db91f576>
- [19] M. A. A. Hammami, N. Raymond, *Nature*, vol. 424, pp. 635–636, 2003.

- [20] F. Torabi and V. Esfahanian, "Study of thermal-runaway in batteries i. theoretical study and formulation," *Journal of The Electrochemical Society*, vol. 158, no. 8, p. A850, 2011. [Online]. Available: <https://doi.org/10.1149/1.3592486>
- [21] Q. Wang, P. Ping, X. Zhao, G. Chu, J. Sun, and C. Chen, "Thermal runaway caused fire and explosion of lithium ion battery," *Journal of Power Sources*, vol. 208, pp. 210–224, 2012. [Online]. Available: <https://www.sciencedirect.com/science/article/pii/S0378775312003989>
- [22] C.-H. Doh, Y.-C. Ha, and S. wook Eom, "Entropy measurement of a large format lithium ion battery and its application to calculate heat generation," *Electrochimica Acta*, vol. 309, pp. 382–391, 2019. [Online]. Available: <https://www.sciencedirect.com/science/article/pii/S0013468619307017>
- [23] S. J. Bazinski and X. Wang, "The influence of cell temperature on the entropic coefficient of a lithium iron phosphate (LFP) pouch cell," *Journal of The Electrochemical Society*, vol. 161, no. 1, pp. A168–A175, dec 2013. [Online]. Available: <https://doi.org/10.1149/2.082401jes>
- [24] M. Dubarry, V. Svoboda, R. Hwu, and B. Y. Liaw, "Incremental capacity analysis and close-to-equilibrium OCV measurements to quantify capacity fade in commercial rechargeable lithium batteries," *Electrochemical and Solid-State Letters*, vol. 9, no. 10, p. A454, 2006. [Online]. Available: <https://doi.org/10.1149/1.2221767>
- [25] Y. Zhao, Y. Patel, T. Zhang, and G. J. Offer, "Modeling the effects of thermal gradients induced by tab and surface cooling on lithium ion cell performance," *Journal of The Electrochemical Society*, vol. 165, no. 13, pp. A3169–A3178, 2018. [Online]. Available: <https://doi.org/10.1149/2.0901813jes>
- [26] J. P. Schmidt, "Verfahren zur charakterisierung und modellierung von lithium-ionen zellen," Ph.D. dissertation, 2013.
- [27] N. Nieto, L. Díaz, J. Gastelurrutia, I. Alava, F. Blanco, J. C. Ramos, and A. Rivas, "Thermal modeling of large format lithium-ion cells," *Journal of The Electrochemical Society*, vol. 160, no. 2, pp. A212–A217, nov 2012. [Online]. Available: <https://doi.org/10.1149/2.042302jes>
- [28] C.-W. Zhang, K.-J. Xu, L.-Y. Li, M.-Z. Yang, H.-B. Gao, and S.-R. Chen, "Study on a battery thermal management system based on a thermoelectric effect," *Energies*, vol. 11, no. 2, 2018. [Online]. Available: <https://www.mdpi.com/1996-1073/11/2/279>
- [29] Y. Hu, S.-Y. Choe, and T. R. Garrick, "Hybridized time-frequency method for the measurement of entropy coefficient of lithium-ion battery," *Electrochimica Acta*, vol. 362, p. 137124, 2020. [Online]. Available: <https://www.sciencedirect.com/science/article/pii/S0013468620315176>
- [30] S. Mendoza, M. Rothenberger, A. Hake, and H. Fathy, "Optimization and experimental validation of a thermal cycle that maximizes entropy coefficient fisher identifiability for lithium iron phosphate cells," *Journal of Power Sources*, vol. 308, pp. 18–28, Mar. 2016.
- [31] P. J. Osswald, M. del Rosario, J. Garche, A. Jossen, and H. E. Hostler, "Fast and accurate measurement of entropy profiles of commercial lithium-ion cells," *Electrochimica Acta*, vol. 177, pp. 270–276, 2015, international Conference on Electrochemical Energy Science and Technology (EEST2014). [Online]. Available: <https://www.sciencedirect.com/science/article/pii/S0013468615002376>
- [32] H. Bhundiya, B. M. Hunt, and B. Drolen, "Measurement of the effective radial thermal conductivities of 18650 and 26650 lithium ion battery cells," in *Thermal and Fluid Analysis Workshop, NASA Jet Propulsion Laboratory, Galveston*, 2018.
- [33] P. Keil, K. Rumpf, and A. Jossen, "Thermal impedance spectroscopy for li-ion batteries with an ir temperature sensor system," in *2013 World Electric Vehicle Symposium and Exhibition (EVS27)*. IEEE, 2013, pp. 1–11.
- [34] G. White, "Peltier Controller User Manual," *Imperial College London*, Nov. 2021.
- [35] B. Earl. Adafruit 4-channel adc breakout. [Online]. Available: <https://learn.adafruit.com/adafruit-4-channel-adc-breakouts/assembly-and-wiring>
- [36] F. Gustafsson, "Determining the initial states in forward-backward filtering," *IEEE Transactions on signal processing*, vol. 44, no. 4, pp. 988–992, 1996.
- [37] Rurwin, "Breadboard jumper-cables acting as antennae." [Online]. Available: <https://forums.raspberrypi.com/viewtopic.php?t=99086>

USER GUIDE

Complete Schematic

The apparatus can be broken down into three sections, with each section compartmentalised and communicating with one another. These sections are broken down below and represented in block model format in Figure 40. See Appendix B in depth labelled images and diagrams of the experimental apparatus and its various sections.

- User Interface (UI)
- Electrical Power & Processing (EPP)
- Heating & Cooling Block (HCB)

The UI is comprised of a 7inch touchscreen LCD interface, powered by the Raspberry Pi. It allows the user to run test, change desired variables and control the system. This is located on the top lid of the box. The two remaining systems are compartmentalised inside the box, separating electrics from heating and liquids.

The HCB is the thermal actuator for running the experiment. It is powered from the electrical power and processing section. The block further contains water cooling loops which are affixed to either side of the block and are fed through via pipes connected to push fit connectors.

The EPP acts as the analogue digital link between the UI and HCB. The EPP includes the ADC bank, the voltage processing and motor controller. The electrical components are affixed to breadboards to allow easy plug in connections, allowing for removal of the Pi.

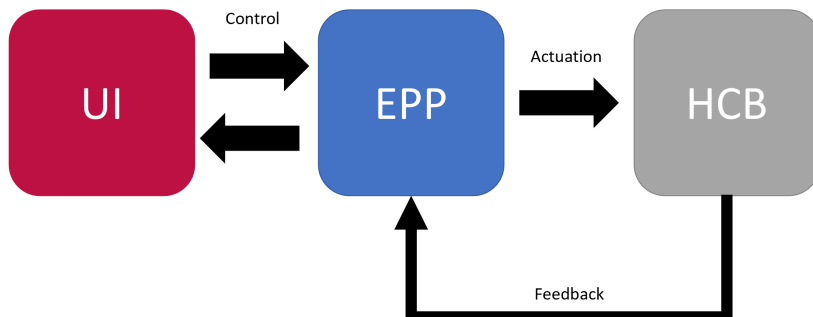


Figure 40: Simple block model showing links between key sections

User Interface

The UI allows data to be extracted from the Pi via the USB ports, it further allows for power supply of fans and the touchscreen, see Figure 41. The purpose of the UI is to communicate with the user and the control system, outputting the commands to the EPP via GPIO pins. The UI connects to the EPP through a connection board in the EPP. For the Physical design, it allows for ease of removal and connection of the Pi from the box. Furthermore it creates a neat and accessible way to create new connections, seen in Appendix B.

The specific connections are shown in Figure 42. These include the I2C connections, providing the data from the ADC bank, and connections to control the motor controller via the connection board. It also connects the kill switch to the Pi, ceasing all operation and cutting power.

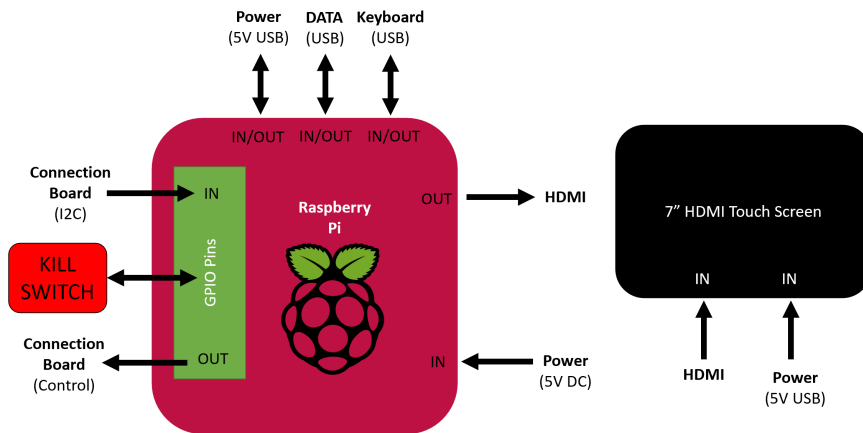


Figure 41: Schematic and connections of the User Interface

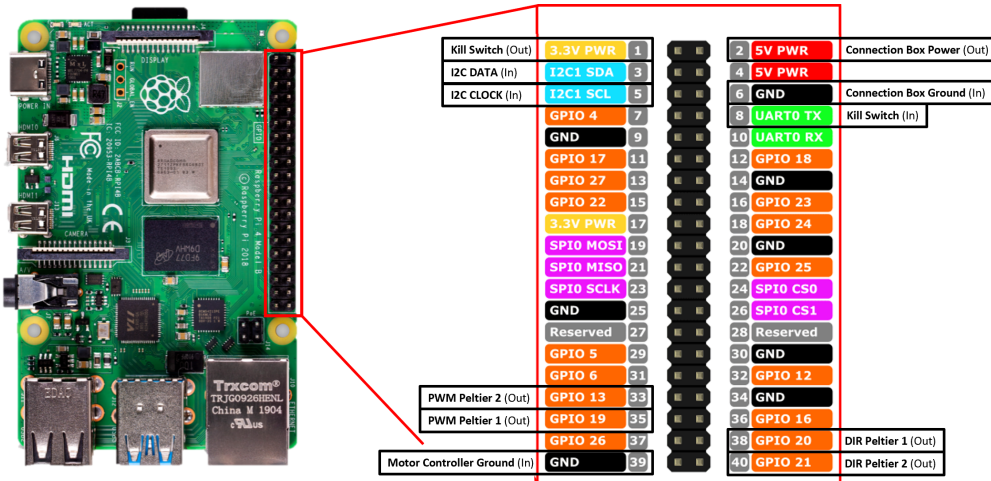


Figure 42: Schematic of GPIO Connections from the PI

Electrical Power & Processing

The EPP is responsible for receiving control signals from the UI, actuating them to the HCB and then receiving, processing and relaying the feedback signals from the HCB back to the UI. See Appendix B for diagrams of box connections.

The connection board links the EPP together; it receives in the Motor Controller control signals, 5V rail power and ADC feedback data, and sends out the signals and power to the relevant blocks. See Figure 43 to reference linked blocks.

The voltage filter is physically located on the lower section of the connection board. It powers the ADC bank with regulated 5V power.

The motor controller is controlled through the connection board but receives its power via fused external connected power supply. It can process a maximum of 300W input, though it is not recommended to reach this power level for safety reasons.

The ADC bank is responsible for processing all the analogue signals of voltage and resistance back to the connection board (via I2C). The breakdown of connections and signals in and out of the block have been broken down in Figure 44. The signals come into the various ADC's, are processed into a bit signal, and then are sent out to the UI via I2C connection.

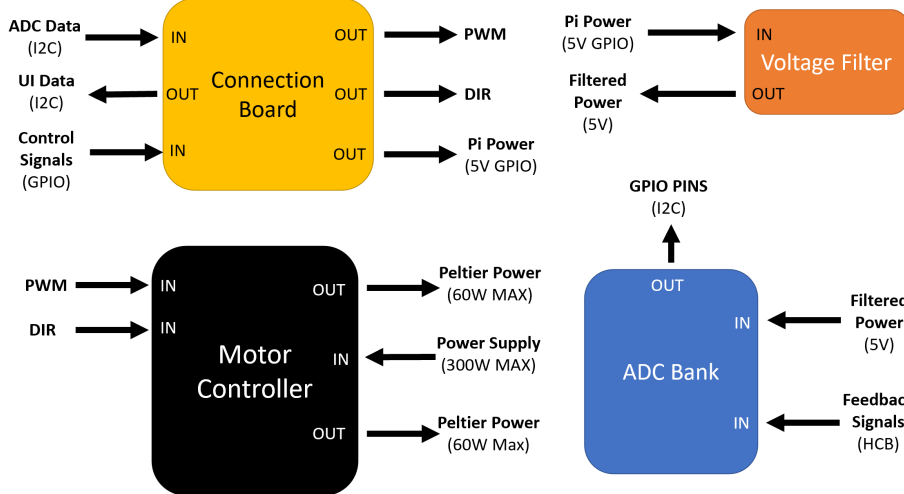


Figure 43: Schematic Electrical Power Processing Compartment

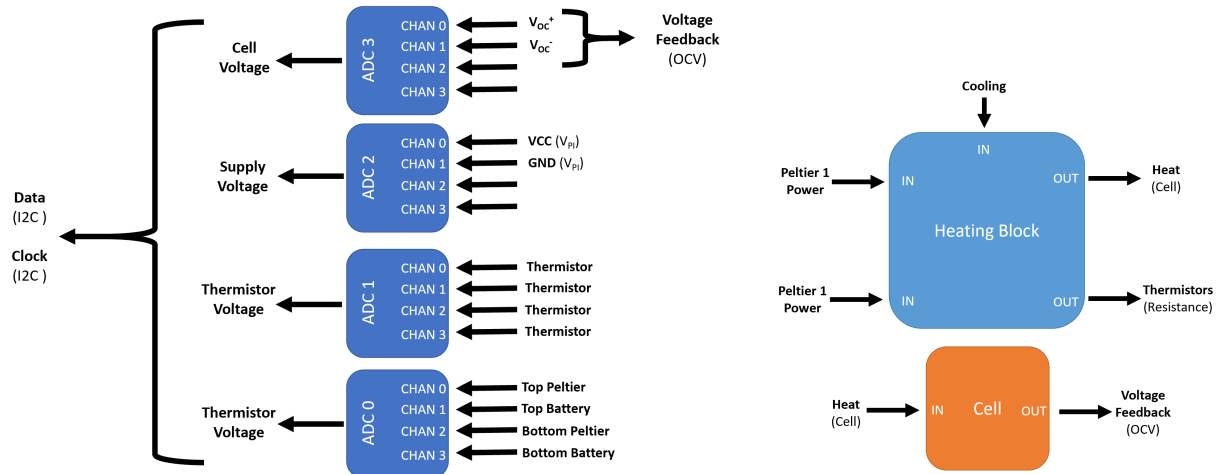


Figure 44: Schematic of individual ADC connections channels

Figure 45: Schematic of Heating and Cooling Block

Heating & Cooling Block

The HCB is the physical actuator of the system and as such uses the power from the EPP, via motor controller, to power the peltiers. These actuate the temperature change within the block and are cooled via external cooler. The cell is thermally interacted by the block and responds with a voltage change, see Figure 45. These thermal and electrical changes are recorded by independent sensors and are fed back to the EPP ADC bank for processing.

User Interface Manual(TG)

This next section will detail the graphical user interface (GUI) and how it is meant to be used. Further details on construction of the GUI code, and how the code might be edited can be found in the appendix.

Start Page

The start page refers to the first screen which the user sees. The safety checklist is a feature which makes sure the users have understood and checked the most safety critical parts of the design. Only when all five of the safety check boxes have been ticked can the user progress to the next page which is the Settings page.

The instructions page is also accessible from here and provides documentation on how to use the device best, as well information on safety.

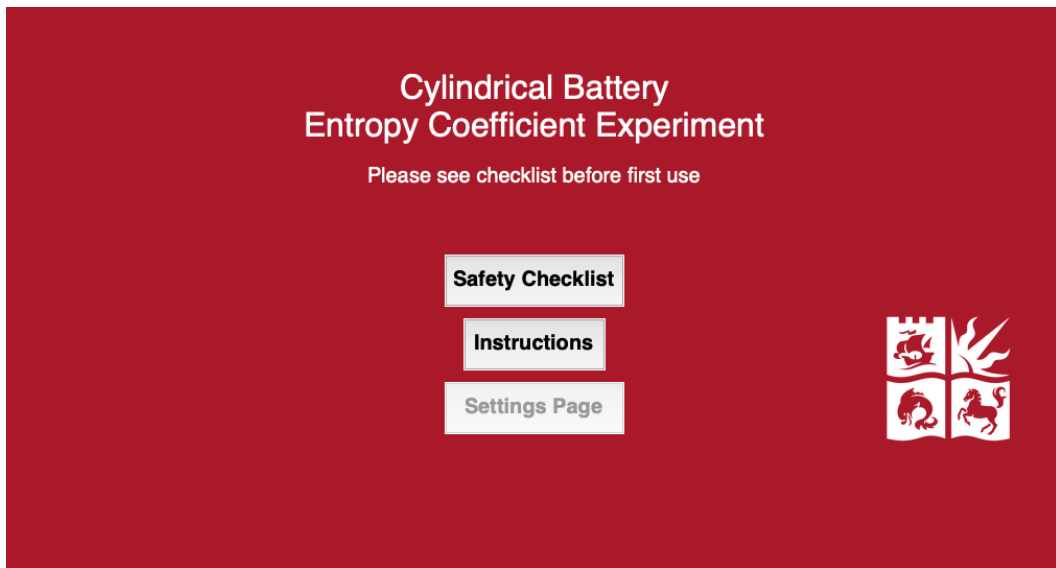


Figure 46: Start page of the GUI

Settings Page

Here the experimental settings can be changed. Command peltiers determines if the peltiers are to be engaged, if this is not selected than no temperature control can occur. A radio button exists to control the method by which the changes in voltage are detected.

In the centre are the numerical settings for the experiment. Each setting comes with it's default value, but if a different value is required then it will take effect on the experiment after the Apply changes button is pressed.

The Start experiment button will run the experiment python file, which begins taking readings and if the command peltiers checkbox is selected it will start heating/cooling the cell. The Start button cannot be pressed until Apply changes has been pressed, and it cannot be pressed twice as this will lead to a race condition, which is where two threads are running the same processes simultaneously causing seemly random and strange errors in output. The Start button is greyed out for the times when it should not be pressed to help prevent these issues.

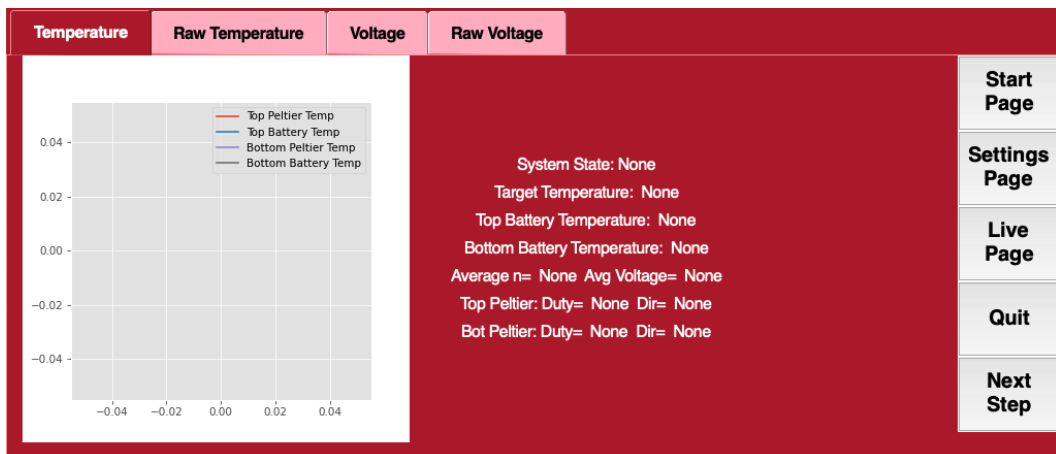


Figure 47: Live page of the GUI

Live Page

This page is where the experiment results can be viewed. The four most relevant metrics are graphed and can be reached by using the tabs at the top of the screen. Temperature and Voltage are plots which contain the moving average data. It should be noted that the graphs for Temperature and Voltage take close to 100 seconds to appear as the moving averages are properly calculated.

The navigation bar can be seen on the right most side of the screen. These are the most important buttons during the experiment and so are visible on both the Settings and Live pages. Aside from the obvious navigation buttons: the Quit button exits the file which runs the peltiers but will not exit the GUI, and the Next step button takes the entropy coefficient measurement and moves the test onto the next temperature step.

Important readouts can be seen in the middle of the screen and they will be continuously updated throughout the experiment.

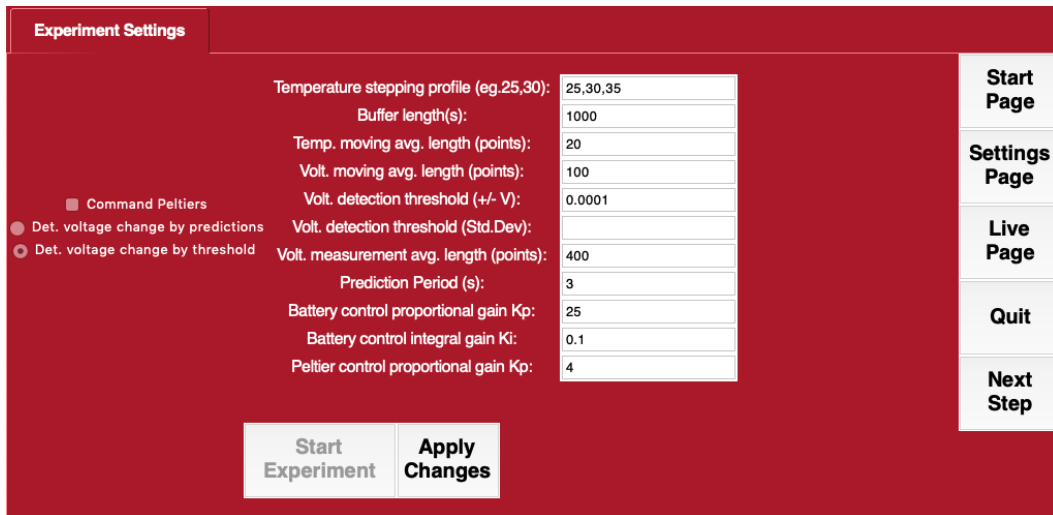


Figure 48: Settings page of the GUI

APPENDIX

Appendix A - Code Structure

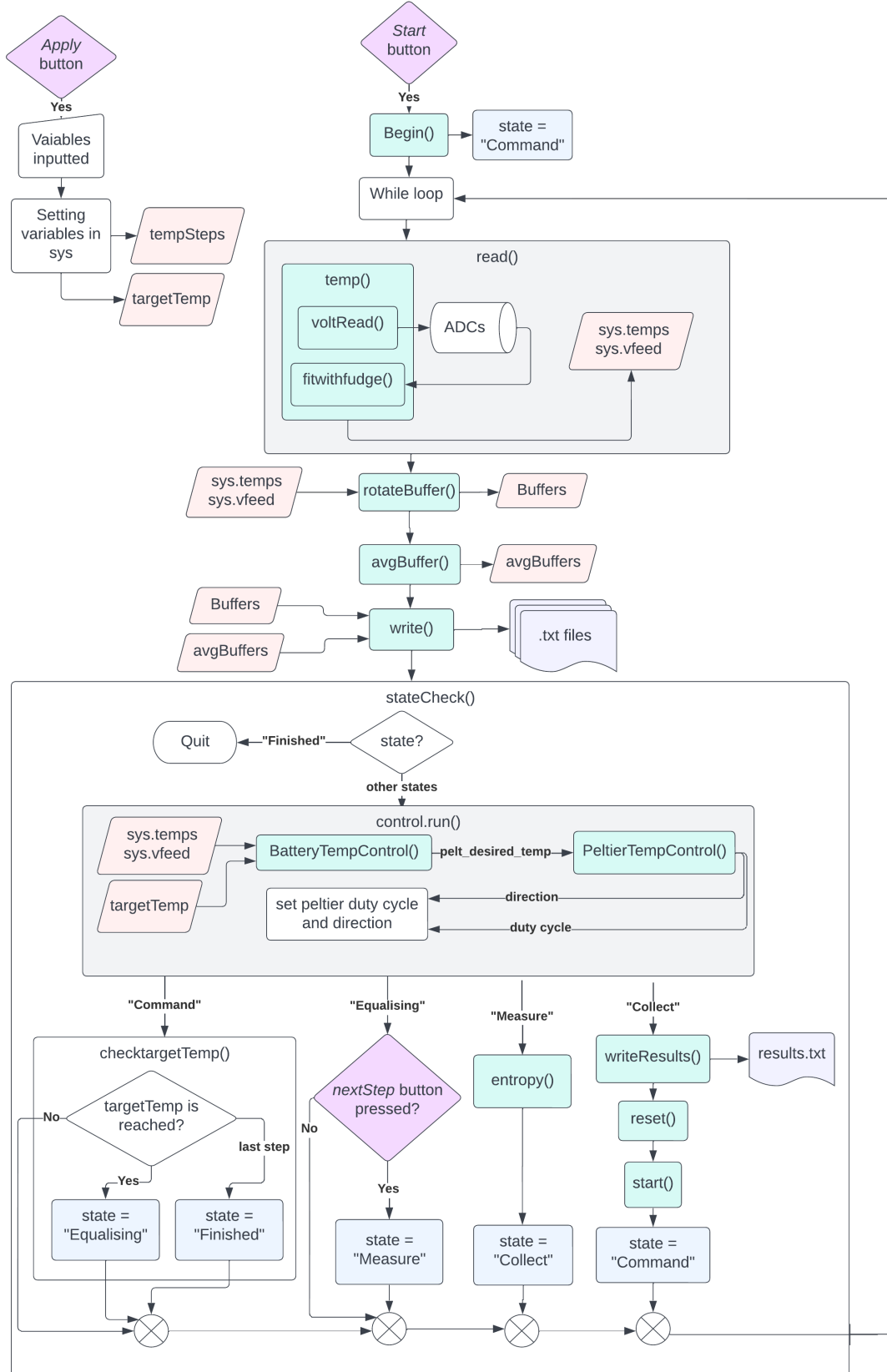


Figure 49: Flow diagram for `EntropyCoefficient.py`

Appendix B - Software Documentation(TG)

Overview

The software for the entropy coefficient experiment is across two files which can be considered as two parts:

- EntropyGUI.py: the GUI as you may have guessed, creates the GUI and then runs the EntropyCoefficient.py file. This file should be run when running the program.
- EntropyCoefficient.py: the main function and system management of the experiment. It initializes all the hardware, reads values and calculates the entropy coefficient etc.

Technical Language

Knowledge of object oriented programming (OOP) in python is assumed throughout this documentation and so keywords such as object, instance and class will be used without explanation.,

The EntropyCoefficient.py file will be discussed first as it introduces the main operation of the experiment.

EntropyCoefficient.py

Overview

The file is broken up into four classes: readVal(), controlPeltiers(), predict(), system(), which house most of the methods, and the main loop is in the runGUI() function.

The object for each class is initialised when the file is first run.

readVal()

This function reads values from all four of the ADC's and converts the voltages into meaningful values, such as temperature and cell voltage. Whenever a fresh reading from the ADC's is required methods in this class are called.

init()

The 4 ADC's are initialised here using an i2c connection (numbered 0,1,2,3), and channels are created for each measurement using the AnalogIN() function.

voltRead() is called to generate initial voltage readings. Voltage readings are stored as attributes in this object.

Nominal resistor values and calibration resistances are read from files I “ResistorNorm.txt” and “ResistorCali.txt” and are set as attributes.

voltRead()

Reads the voltages from all the channels. Vnorm is the voltage measurement from the pi 5V line. Vfeed is the voltage from the cell, and Vsens is a numpy array of the voltages from the temperature reading channels.

resist()

Calculates the resistance of each thermistor given Vsens

fitwithFudge()

Calculates a temperature from a thermistor resistance, res and a calibration resistance, res0.

temp()

Calls voltRead() to read the voltages from the ADC and then combines resist() and fitwithfudge() to get a vector of temperatures, which it stores as an attribute. This is the method which is called when other classes need fresh voltage temperature readings. It is called at the beginning of a “tick” and the results are used by the rest of the classes at the current temperature and voltage readings.

controlPeltiers()

This class has methods for controlling the peltiers.

init()

The pins on the pi which control the peltiers are initialized. The peltiers are set to off (duty cycle = 0) initially.

run()

This method is called when the peltiers are commanded to a certain temperature. The current temperature step (desired_temp) is passed as an argument along with the current temperature readings for the peltiers and cell.

sys.commandPeltier is initialised as 0 and only becomes 1 when the appropriate box is checked in the settings page of the GUI. This stops the peltiers from commanding the first temperature step immediately.

If sys.commandPeltier == 1 the peltiers are controlled. BatteryTemperatureControl() is called and returns the peltier desired temperature, which is fed into PeltierTempControl() to get the peltier directions and duty cycles.

Safety features have been added here to make sure that the peltier temperature which is commanded is never above 50 or below 5 degrees. The 5 degrees limit is there to stop condensation forming on the block and potentially creating a short circuit across the cell.

The functions ChangeDutyCycle() and GPIO.output() are used to set the desired duty cycles and directions of the peltiers.

BatteryTempControl()

This function takes the desired cell temperature and the current cell temperature, generates an error and applies PI control to produce a desired peltier temperature.

PeltierTempControl()

Here the error is simply the peltier_desired_temp which is passed by BatteryTempControl() as this was found to generate appropriate dutycycles. Only proportional gain is applied here. If statements are here to rectify the direction of the peltiers when the error changes sign. Changing direction in the peltiers will command them to switch modes from heating-cooling and back again.

Predict()

This class contains the methods which are required to generate voltage predictions during an experiment. Theoretically the change in voltage for a single temperature step follows an exponential decay, and so its path can be predicted which could potentially provide an accurate guess for the final voltage of the cell, shortening the amount of time required.

This functionality has been built but has had only limited testing. The methods will be described here and the intentional functionality will be described, but they may not behave as intended.

init()

derGap is the amount of points over which the derivative is calculated. FinalPredictions is a list which will contain all of the predictions made.

waitToPredict()

simply waits 5 seconds. This is so that the last temperature step has a chance to effect the cell temperature before the predictStart() function begins to try find a point where the predictions can be started from.

The appropriate time to wait is not known as proper testing was not carried out.

predictStart()

The exponential() function cannot curve fit exponential curves if the data contains features which are due to other effects, such as the gentle increase in temperature as the cell initially begins to heat up. This function finds the point in the last X values of temperature which has the highest gradient as this represents (in theory) the beginning of the exponential decay of the voltage. This function finds that point and returns the time at which it occurs so that the data which is passed onto the exponential() function can be cut accordingly.

To calculate the derivative a second list of the voltages, vBuffAvg is made and the values are moved along by X places (default is 5) , vBuffAvgShift then these lists are taken away from eachother to give a list which represents the changes of voltages over 5 ticks of data, delta. Every 5th element of delta is taken and the corresponding values of time are taken, timeDelta. The largest value in the vector of the changes in voltage, max(diff), gives the point with the maximum derivative, and the time which this happens is returned from the function

cutData()

This function takes the buffers for raw voltage and time and truncates them at the point found by predictStart(). These will be the lists which are used by the exponential() function, vBuffCut and timeBuffCut

Exponential()

vBuffCut is put through a low pass filter and then curve_fit. This curve is then used to generate mock X and Y coordinates for the guess, and to do this it is evaluated against a timeseries of 0,20001, this is so that a number very close to the asymptotic limit is obtained. The final value of the curve fit, and the guess from this function is curveY[20000] and this value is appended to the finalPredictions list which was created in _init_()

sDeviation()

With every prediction that is made the last 3 predictions are analyzed by this function to determine if they are close enough to each other to be used as a value in the calculations.

The last predictions meet this criteria when the standard deviation of the predictions is less than a threshold (default is 1e-5). Then the system state is changed so that it can move into the measure state, and sys.entropy() is called. The predicted value is the average of the 3 values which were analysed for the standard deviation.

system()

This class governs all the others, it contains the methods which control the actions of the experiment and it's interaction with the GUI.

setBuffer()

The buffers are deques which hold the last x points of data for the 4 most important temperatures, the time, and the voltage of the cell. Deques were used because they have very quick operations to remove and add datapoints, although it is thought that the overall speed of the program may be degreased as a result of using deques because they often have to be converted to other datatypes, for example a numpy array in movingAverage().

It's important to have construct like the deque so that lists are not indefinitely growing in size whilst the program is running.

In this function the deques are initialised, they are appended and rotated later.

usrStepChoice()

This function takes the string of temperature steps which is inputted by the user in the GUI and turn it into a list of integer values called tempSteps which is used many times in system() to control the experiment.

read()

This calls the read class and sets the results to attributes. Temps are a list of all the temperatures from the sensor, and vfeed is the voltage from the cell.

rotateBuffer()

This function takes the buffers and updates them. The oldest values in the buffer are removed and the newest values are added at the front.

write()

Each tick this function is called and it writes self.temps and vfeed to the Data.txt file. And then it writes the average temps and average voltage to the MovingData.txt file. The columns for both these files are: Seconds — top peltier temp — top battery temp — bot peltier temp — bot battery temp — cell voltage

writeResults()

After the entropy coefficient is calculated this function is called to write the experiment results to the file ResultsData.txt file. The columns in this file are: Last temp step — current temp step — entropy coefficient — final voltage — last avg voltage — total seconds

averageBuffer()

Calls the movingAverage() function on each buffer to give averaged versions of them. This is only done after a certain time period as it's best if the moving average function is calculated once the buffer has filled up following the initial start-up period. This is because 0 initial values in the buffer will skew the moving average calculations.

clearFile()

This is run at the beginning of the program as this clears the data.txt and movingData.txt files. If there was data from a previous experiment in there it will be destroyed, so any experimental data should be saved before a new experiment has started.

timeLog()

This function takes the start and end times for a single tick, which are found using the .time library, and adds it to the running float value of seconds. This is the time used for plotting and any calculations.

stateCheck()

This is the main controller function. The different jobs that the code is expected to do are separated here into states. The states are: Command, Equalising, Measure, Collect, and Finished. All of them will be described in detail below, but first a few notes about all of the states.

All the states apart from Finished command the peltiers. This is because this required for the cell temperature to be controlled. All of these states will command the cell temperature to be at the current targetTemp, this temperature may be changed at points but they will always command to the current targetTemp.

Command This state is used just after a new temperature step has been commanded. It represents the time when the temperature of the cell is increasing towards the new desired temperature.

If voltage prediction is requested by the user via the settings page in the GUI the predictStart = 1, and the voltage predictions will begin here. This includes all the methods described in the predict class. This section of the code has had little testing and it is not recommended that It is used without development. By default voltage prediction is not requested.

checktargetTemp() is called to check weather the temperature has been reached. If it has then the state is changed to Equalising.

Equalising This represents the time where the outside cell temperature has been reached but the cell is still thermally and chemically equalising. This is the crucial and time consuming period for most entropy coefficient experiments as it is important for cell voltage to equalise before it is measured.

Currently voltageLevel() is not used, which is a function that detects when the change in voltage has dropped to a minimum. Instead the program state will remain as Equalising until the Next Step button is pressed by the user, if it is pressed the state will become Measure

Measure This state is when the entropy coefficient is being measured. This only takes one tick so it's a very short lived state. Entropy() is called and sets the next state to Collect

Collect In this state the loose ends from the last temperature step are dealt with. The results of the measurement are written by writeResults(). Reset() sets all the important attributes so that they can be used again in the next entropy coefficient measurement. Start() sets the targetTemp for the next step and sets the system state back to Command. If this temperature step is the last one the next state is set to Finished.

Finished This is the final state and it quits the EntropyCoefficient.py file

voltageLevel()

This checks to see if the last two average voltages are within the range voltLevelRange. If this is the case then the voltage system state is set to Measure

forceStep()

This function is called by the GUI when the Next Step button is pressed, it sets the next state to Measure it's used instead of voltageLevel() to determine when the entropy coefficient should be measured.

start()

Is called in the Collect state and it updates the targetTemp. It detects if the current step is the last step and sets the state to Finished. If it's not the last step the state is set to Command.

checkTargetTemp()

If there is ± 0.1 degree difference between both the average cell temperatures, `temp1Avg[0]` `temp3Avg[0]` and the target temp then this function will set the state to Equalising.

entropy()

Takes an average of the last `voltMeasureLen` points of `vBuffAvg` to get a more accurate measurement of the voltage than simply one of the moving average points from `vBuffAvg`.

The temperature measurement is taken as the difference between the current measured temperatures and the previous step.

The entropy coefficient is just the division of the change in voltage by the change in temperature.

reset()

sets the `lastVoltage` to the current voltage for the next steps entropy coefficient measurement.

The integral error counters are set to 0 Resets the `predictStart` variable to “wait” which indicates that the predictions should wait to start making predictions. (not relevant in current code)

off()

When triggered this will set the peltier elements to stop heating and it quits the `EntropyCoefficient.py` file.

buttonCheck()

This checks the physical button which was implemented to see if it's been pressed. If it has then it quits the `EntropyCoefficient.py` file

measureStartTime()

Measures the time at the beginning of a tick.

measureEndTime()

Measures the time at the end of a tick.

Appendix C - Apparatus Diagrams

